

**DEVELOPMENT OF COMPUTER PROGRAM FOR
PREDICTING CONFIGURATIONS OF SOLUTION
CAVERNS ON TOP OF SALT BED**

Sarayuth Aracheeploha

A Thesis Submitted in Partial Fulfillment of the Requirements for the

Degree of Master of Engineering in Geotechnology

Suranaree University of Technology

Academic Year 2009

การพัฒนาโปรแกรมคอมพิวเตอร์เพื่อคาดคะเนลักษณะของ
โพรงละลายบนชั้นเกลือหิน

นายสรายุทธ อาชีพโลหะ

วิทยานิพนธ์นี้เป็นส่วนหนึ่งของการศึกษาตามหลักสูตรปริญญาวิศวกรรมศาสตรมหาบัณฑิต

สาขาวิชาเทคโนโลยีธรณี

มหาวิทยาลัยเทคโนโลยีสุรนารี

ปีการศึกษา 2552

**DEVELOPMENT OF COMPUTER PROGRAM FOR PREDICTING
CONFIGURATIONS OF SOLUTION CAVERNS
ON TOP OF SALT BED**

Suranaree University of Technology has approved this thesis submitted in partial fulfillment of the requirements for the Master's degree.

Thesis Examining Committee

(Asst. Prof. Thara Lekuthai)

Chairperson

(Assoc. Prof. Dr. Kittitep Fuenkajorn)

Member (Thesis Advisor)

(Dr. Prachaya Tepnarong)

Member

(Prof. Dr. Pairote Sattayatham)

Vice Rector for Academic Affairs

(Assoc. Prof. Dr. Vorapot Khompis)

Dean of Institute of Engineering

สรายุทธ อาชีพโลหะ : การพัฒนาโปรแกรมคอมพิวเตอร์เพื่อคาดคะเนลักษณะของ
โพรงละลายบนชั้นเกลือหิน (DEVELOPMENT OF COMPUTER PROGRAM FOR
PREDICTING CONFIGURATIONS OF SOLUTION CAVERNS ON TOP OF
SALT BED) อาจารย์ที่ปรึกษา : รองศาสตราจารย์ ดร.กิตติเทพ เฟื่องขจร, 98 หน้า.

วิธีการวิเคราะห์ชุดหนึ่งได้ถูกพัฒนาขึ้นเพื่อคาดคะเนตำแหน่ง ความลึก และขนาดของ
โพรงที่ถูกละลายขึ้นที่รอยต่อระหว่างชั้นเกลือและชั้นหินปิดทับ สมการควบคุมแบบไฮเปอร์
โบลิก ได้ใช้ในการวิเคราะห์เชิงสถิติของข้อมูลสำรวจผิวดินเพื่อกำหนดตำแหน่งของโพรง ค่า
ทรุดตัวสูงสุดของผิวดิน ค่าความเอียงสูงสุด และค่าความโค้งสูงสุดภายใต้สภาวะต่ำกว่าจุด
วิกฤต และที่จุดวิกฤตของการทรุดตัว โปรแกรมคอมพิวเตอร์ได้ถูกพัฒนาขึ้นเพื่อใช้ในการ
วิเคราะห์นี้ซึ่งจะให้ค่าองค์ประกอบการทรุดตัวและลักษณะการทรุดตัวที่สามารถใช้เป็น
ตัวแทนภายใต้สภาวะต่ำกว่าจุดวิกฤต และที่จุดวิกฤต การวิเคราะห์ด้วยระเบียบวิธีเชิงตัวเลข
โดยใช้โปรแกรม FLAC สามารถสร้างความสัมพันธ์ระหว่างองค์ประกอบของการทรุดตัวกับ
ขนาดและความลึกของโพรงโดยมีการผันแปรความแข็งและความยืดหยุ่นของชั้นหินปิดทับเข้า
มาพิจารณาด้วย ผลที่ได้คือชุดของสมการความสัมพันธ์ที่เชื่อมระหว่างองค์ประกอบของการ
ทรุดตัวกับคุณลักษณะของโพรงและคุณสมบัติของชั้นหินปิดทับ การศึกษาภายใต้สภาวะที่เกิน
กว่าจุดวิกฤตได้ใช้ระเบียบวิธีเชิงตัวเลข (โปรแกรม UDEC) และแสดงให้เห็นว่าความไม่
แน่นอนของการเคลื่อนตัวของชั้นหินปิดทับ และการเกิดหลุมยุบจะเป็นผลมาจากความ
ซับซ้อนของการเปลี่ยนรูปร่างของหินหลังจากเกิดการแตกและการเคลื่อนตัวของรอยแตก
ที่มีอยู่ก่อนในชั้นหินปิดทับ ความสัมพันธ์ระหว่างองค์ประกอบของการทรุดตัวกับคุณสมบัติ
เชิงกลศาสตร์ของชั้นหินปิดทับและรูปทรงเรขาคณิตของโพรงนั้นจะสามารถนำมาประยุกต์ใช้
ในพื้นที่ที่มีคุณสมบัติภายในขอบเขตของงานวิจัยนี้ (อาทิ โพรงมีรูปร่างครึ่งรูปไข่เกิดขึ้นที่
รอยต่อระหว่างชั้นหินปิดทับและชั้นเกลือ ชั้นหินอยู่ในแนวระนาบ ผิวดินมีความเรียบ
สม่ำเสมอ และชั้นหินปิดทับอึดตัวด้วยน้ำเกลือ) ผลจากงานวิจัยนี้อาจไม่สามารถนำมา
ประยุกต์ใช้ในกรณีที่การทรุดตัวเกิดจากลักษณะของชั้นหินและรูปร่างของโพรงที่ต่างไปจาก
งานวิจัยนี้ วิธีที่เสนอมานี้จะไม่สามารถนำมาประยุกต์ใช้ภายใต้สภาวะเกินกว่าจุดวิกฤต ที่ซึ่ง
พฤติกรรมหลังการพังทลายของชั้นหินปิดทับไม่สามารถคาดคะเนได้และมีความซับซ้อนด้วย
ระบบของรอยแตกที่มีอยู่ก่อน ดังแสดงให้เห็นจากผลของระเบียบวิธีเชิงตัวเลข อย่างไรก็ตาม

วิธีที่เสนอในงานวิจัยนี้สามารถนำมาใช้ในการหารูปร่างของโพรง และองค์ประกอบของการ
ทรุดตัวที่เกิดขึ้นจากการสูบน้ำเกลือ ดังนั้นวิธีการแก้ไขสามารถดำเนินการได้ทัน่วงทีเพื่อลด
ผลกระทบที่เกิดจากโพรงใต้ดินก่อนที่จะเกิดการทรุดตัวอย่างรุนแรงหรือหลุมยุบบนผิวดิน

SARAYUTH ARACHEEPLOHA : DEVELOPMENT OF COMPUTER
PROGRAM FOR PREDICTING CONFIGURATIONS OF SOLUTION
CAVERNS ON TOP OF SALT BED. THESIS ADVISOR : ASSOC. PROF.
KITTITEP FUENKAJORN, Ph.D., PE., 98 PP.

SUBSIDENCE/CAVERN/SOLUTION/SINKHOLE/SALT

An analytical method has been developed to predict the location, depth and size of caverns created at the interface between salt and overlying formations. A governing hyperbolic equation is used in a statistical analysis of the ground survey data to determine the cavern location, maximum subsidence, maximum surface slope and surface curvature under the sub-critical and critical conditions. A computer program is developed to perform the regression and produce a set of subsidence components and a representative profile of the surface subsidence under sub-critical and critical conditions. Finite difference analyses using FLAC code correlate the subsidence components with the cavern size and depth under a variety of strengths and deformation moduli of the overburden. Set of empirical equations correlates these subsidence components with the cavern configurations and overburden properties. For the super-critical condition a discrete element method (using UDEC code) is used to demonstrate the uncertainties of the ground movement and sinkhole development resulting from the complexity of the post-failure deformation and joint movements in the overburden. The correlations of the subsidence components with the overburden mechanical properties and cavern geometry are applicable to the range of site conditions specifically imposed here (e.g., half oval-shaped cavern created at

the overburden-salt interface, horizontal rock units, flat ground surface, and saturated condition). These relations may not be applicable to subsidence induced under different rock characteristics or different configurations of the caverns. The proposed method is not applicable under super-critical conditions where post-failure behavior of the overburden rock mass is not only unpredictable but also complicated by the system of joints, as demonstrated by the results of the discrete element analyses. The proposed method is useful as a predictive tool to identify the configurations of a solution cavern and the corresponding subsidence components induced by the brine pumping practices. Subsequently, remedial measure can be implemented to minimize the impact from the cavern development before severe subsidence or sinkhole occurs.

School of Geotechnology

Academic Year 2009

Student's Signature_____

Advisor's Signature_____

ACKNOWLEDGEMENTS

The author wishes to acknowledge the support from the Suranaree University of Technology (SUT) who has provided funding for this research.

Grateful thanks and appreciation are given to Assoc. Prof. Dr. Kittitep Fuenkajorn, thesis advisor, who lets the author work independently, but gave a critical review of this research. Many thanks are also extended to Asst. Prof. Thara Lekuthai and Dr. Prachaya Tepnarong, who served on the thesis committee and commented on the manuscript.

Finally, I most gratefully acknowledge my parents and friends for all their supported throughout the period of this research.

Sarayuth Aracheeploha

TABLE OF CONTENTS

| | Page |
|---|----------|
| ABSTRACT (THAI) | I |
| ABSTRACT (ENGLISH)..... | III |
| ACKNOWLEDGEMENTS | V |
| TABLE OF CONTENTS..... | VI |
| LIST OF TABLES | IX |
| LIST OF FIGURES | X |
| LIST OF SYMBOLS AND ABBREVIATIONS..... | XIV |
| CHAPTER | |
| I INTRODUCTION | 1 |
| 1.1 Rationale and background | 1 |
| 1.2 Research objectives | 2 |
| 1.3 Scope and limitations | 3 |
| 1.4 Research methodology | 3 |
| 1.5 Thesis contents | 5 |
| II LITERATURE REVIEW | 6 |
| 2.1 Introduction | 6 |
| 2.2 Rock salt in northeast region of Thailand | 6 |
| 2.3 Site conditions | 9 |

TABLE OF CONTENTS (Continued)

| | Page |
|--|-----------|
| 2.4 Calculation of surface subsidence | 12 |
| 2.4.1 Theory and criterion | 12 |
| 2.4.2 Calculation with SALT_SUBSID program | 14 |
| 2.4.3 FLAC program | 15 |
| III NUMERICAL SIMULATIONS | 17 |
| 3.1 Introduction | 17 |
| 3.2 Finite difference simulations | 17 |
| 3.3 Results | 19 |
| 3.4 Profile function | 24 |
| IV MATHEMATICAL RELATIONSHIPS | 33 |
| 4.1 Introduction | 33 |
| 4.2 Statistical analysis of the ground survey data | 33 |
| 4.3 Empirical equations | 38 |
| 4.4 Example of calculation | 43 |
| 4.5 Super – critical condition | 48 |
| 4.6 Discrete element analysis | 49 |
| 4.7 Field investigations | 55 |
| V CONCLUSIONS AND RECOMMENDATIONS | 59 |
| 5.1 Conclusions | 59 |
| 5.2 Recommendations | 60 |

TABLE OF CONTENTS (Continued)

| | Page |
|--------------------------------|------|
| REFERENCES..... | 61 |
| APPENDICES | |
| APPENDIX A SOURCE CODE..... | 66 |
| APPENDIX B USER MANUAL..... | 77 |
| APPENDIX C PUBLICATION..... | 80 |
| BIOGRAPHY | 98 |

LIST OF TABLES

| Table | | Page |
|--------------|---|-------------|
| 3.1 | Variables used in FLAC simulations. The deformation moduli (E_m) vary from 20, 40, 60 to 80 MPa and friction angle (ϕ) vary from 20°, 40° to 60° | 20 |
| 4.1 | Example of ground survey data measured in subsiding area | 47 |

LIST OF FIGURES

| Figure | | Page |
|--------|---|------|
| 1.1 | Research methodology | 4 |
| 2.1 | Sakon Nakhon and Khorat Basins containing rock salt in the northeast of Thailand..... | 7 |
| 2.2 | Cross-section showing rock salt in the Khorat Basin..... | 10 |
| 2.3 | Brine pumping areas in Khorat and Sakon Nakhon salt basins..... | 10 |
| 3.1 | Example of finite difference mesh used in FLAC simulation. Analysis is made in axial symmetry. $H = 5$ m, $d = 60$ m, $w = 60$ m, $B = 172$ m, $E_m = 40$ MPa and $\phi = 20^\circ$ | 18 |
| 3.2 | The maximum subsidence (S_{max}) from FLAC simulations. $d = 40$ m and $H = 5$ m. | 21 |
| 3.3 | The maximum subsidence (S_{max}) from FLAC simulations. $d = 50$ m and $H = 5$ m. | 21 |
| 3.4 | The maximum subsidence (S_{max}) from FLAC simulations. $d = 60$ m and $H = 5$ m. | 22 |
| 3.5 | The maximum subsidence (S_{max}) from FLAC simulations. $d = 70$ m and $H = 5$ m. | 22 |
| 3.6 | The maximum subsidence (S_{max}) from FLAC simulations. $d = 80$ m and $H = 5$ m. | 23 |

LIST OF FIGURES (Continued)

| Figure | Page |
|--------|---|
| 3.7 | FLAC simulations compared with hyperbolic function calculations for $\phi = 20^\circ$, $E_m = 20$ MPa, $d = 40$ m and $w = 40$ m 27 |
| 3.8 | FLAC simulations compared with hyperbolic function calculations for $\phi = 20^\circ$, $E_m = 40$ MPa, $d = 40$ m and $w = 40$ m 28 |
| 3.9 | FLAC simulations compared with hyperbolic function calculations for $\phi = 20^\circ$, $E_m = 60$ MPa, $d = 40$ m and $w = 40$ m 29 |
| 3.10 | FLAC simulations compared with hyperbolic function calculations for $\phi = 20^\circ$, $E_m = 20$ MPa, $d = 60$ m and $w = 40$ m 30 |
| 3.11 | FLAC simulations compared with hyperbolic function calculations for $\phi = 20^\circ$, $E_m = 40$ MPa, $d = 60$ m and $w = 40$ m 31 |
| 3.12 | FLAC simulations compared with hyperbolic function calculations for $\phi = 20^\circ$, $E_m = 60$ MPa, $d = 60$ m and $w = 40$ m 32 |
| 4.1 | Variables used in this study 34 |
| 4.2 | Regression of ground survey data (top) to obtain a representative hyperbolic profile of ground surface (bottom). Vertical scale is greatly exaggerated 37 |
| 4.3 | Maximum slope to critical cavern width ratio (G/w_{cri}) as a function of friction angle (ϕ) for various deformation moduli (E_m). A_0 , B_0 , α_{A0} , β_{A0} , α_{B0} and β_{B0} are empirical constants..... 39 |

LIST OF FIGURES (Continued)

| Figure | Page |
|--|------|
| 4.4 Cavern depth to critical cavern width ratio (d/w_{cri}) as a function of deformation modulus (E_m) for various friction angles (ϕ). A_1 , B_1 , α_{A1} , β_{A1} , α_{B1} and β_{B1} are empirical constants..... | 40 |
| 4.5 Roof deformation to maximum subsidence ratio at critical condition ($R_s/S_{max, cri}$) as a function of deformation modulus (E_m) for various friction angles. A_2 , B_2 , α_{A2} , β_{A2} , α_{B2} and β_{B2} are empirical constants..... | 41 |
| 4.6 Diameter of influence to critical cavern width ratio (B/w_{cri}) as a function of deformation modulus (E_m) for various friction angles. A_3 , B_3 , α_{A3} , β_{A3} , α_{B3} and β_{B3} are empirical constants..... | 42 |
| 4.7 Maximum slope to cavern width ratio (G/w) as a function of maximum subsidence (S_{max}) for various deformation moduli (E_m). A_4 , B_4 , α_{A4} , β_{A4} , α_{B4} and β_{B4} are empirical constants..... | 44 |
| 4.8 Cavern depth to cavern width ratio (d/w) as a function of maximum slope (G) for various deformation moduli (E_m). A_5 , B_5 , α_{A5} , β_{A5} , α_{B5} and β_{B5} are empirical constants..... | 45 |
| 4.9 Ratio of roof deformation to cavern width ratio (R_s/w) as a function of maximum subsidence (S_{max}) for various deformation moduli (E_m). A_6 , B_6 , α_{A6} , β_{A6} , α_{B6} and β_{B6} are empirical constants..... | 46 |
| 4.10 UDEC simulations for cavern roof failure for joints with friction angles of 20° (top), 30° (middle) and 40° (bottom). $H = 30$ m, $d = 40$ m, $w = 100$ m..... | 50 |

LIST OF FIGURES (Continued)

| Figure | Page |
|---|------|
| 4.11 UDEC simulations for cavern roof failure with joint dip angles of 45° (top), 30° (middle) and 15° (bottom). H = 30 m, d = 40 m, w = 100 m..... | 52 |
| 4.12 UDEC simulations for cavern roof failure with cavern diameter of 50 m (top), 75 m (middle) and 100 m (bottom). H = 30 m, d = 40 m, joint dip = 45° | 53 |
| 4.13 UDEC simulations for cavern roof failure with cavern height of 10 m (top), 20 m (middle) and 30 m (bottom). d = 40 m, w = 100 m, joint dip = 45° | 54 |
| 4.14 Some sinkhole caused by brine pumping at Nonsabaeng village, Banmuang district, Sakon Nakhon..... | 56 |
| 4.15 Some sinkhole caused by brine pumping at Nonsabaeng village, Banmuang district, Sakon Nakhon..... | 57 |
| 4.16 Some very big sinkhole caused by brine pumping at Nonsabaeng village, Banmuang district, Sakon Nakhon..... | 58 |

LIST OF SYMBOLS AND ABBREVIATIONS

| | | |
|-------|---|---|
| A_0 | = | empirical constant for equation (4.5) |
| a_0 | = | Half of the maximum subsidence (S_{\max}) |
| A_1 | = | empirical constant for equation (4.6) |
| a_1 | = | Scaling factor |
| A_2 | = | empirical constant for equation (4.7) |
| a_2 | = | Planar offset |
| A_3 | = | empirical constant for equation (4.8) |
| a_3 | = | Vertical offset |
| a_4 | = | $\Sigma x_i/n$ |
| A_4 | = | empirical constant for equation (4.9) |
| a_5 | = | $\Sigma y_i/n$ |
| A_5 | = | empirical constant for equation (4.10) |
| A_6 | = | empirical constant for equation (4.11) |
| b | = | Constant |
| B | = | Maximum radius of cavern area |
| $B/2$ | = | Radius of influence |
| B_0 | = | empirical constant for equation (4.5) |
| B_1 | = | empirical constant for equation (4.6) |
| B_2 | = | empirical constant for equation (4.7) |
| B_3 | = | empirical constant for equation (4.8) |

LIST OF SYMBOLS AND ABBREVIATION (Continued)

| | | |
|-----------|---|---|
| B_4 | = | empirical constant for equation (4.9) |
| B_5 | = | empirical constant for equation (4.10) |
| B_6 | = | empirical constant for equation (4.11) |
| c | = | Arbitrary constant |
| d | = | Cavern depths |
| D | = | Depth of cavern |
| E | = | Extraction ratio of the mine |
| E_m | = | Deformation modulus |
| G | = | Maximum slope |
| $G(x)$ | = | Slope |
| H | = | Cavern height |
| N | = | Model parameters |
| r_i | = | Distance from data point 'i' to the center of the group of data |
| R_s | = | Roof deformation |
| $S(r_i)$ | = | subsidence magnitude at point 'i', where i varied from 1 to the total number of measurements, n) |
| $S(x)$ | = | Vertical displacement |
| S_{max} | = | Maximum subsidence |
| t | = | Time since excavation |
| $u(x)$ | = | Horizontal displacement |
| w | = | Cavern diameters |
| w_{cri} | = | Critical cavern diameters |

LIST OF SYMBOLS AND ABBREVIATION (Continued)

| | | |
|---------------|---|---|
| x | = | Horizontal distance |
| x_i | = | Coordinates of subsidence measured at point 'i' |
| y_i | = | Coordinates of subsidence measured at point 'i' |
| Y_o | = | Model parameters |
| Y_{ss} | = | Model parameters |
| z | = | Vertical displacements of the ground surface |
| Z_u | = | Ultimate surface displacement at any location |
| γ | = | Angle of draw |
| β | = | Model parameters |
| α_{A0} | = | empirical constant for equation (4.5) |
| α_{A1} | = | empirical constant for equation (4.6) |
| α_{A2} | = | empirical constant for equation (4.7) |
| α_{A3} | = | empirical constant for equation (4.8) |
| α_{A4} | = | empirical constant for equation (4.9) |
| α_{A5} | = | empirical constant for equation (4.10) |
| α_{A6} | = | empirical constant for equation (4.11) |
| α_{B0} | = | empirical constant for equation (4.5) |
| α_{B1} | = | empirical constant for equation (4.6) |
| α_{B2} | = | empirical constant for equation (4.7) |
| α_{B3} | = | empirical constant for equation (4.8) |
| α_{B4} | = | empirical constant for equation (4.9) |
| α_{B5} | = | empirical constant for equation (4.10) |

LIST OF SYMBOLS AND ABBREVIATION (Continued)

| | | |
|------------------|---|--|
| α_{B6} | = | empirical constant for equation (4.11) |
| β_{A0} | = | empirical constant for equation (4.5) |
| β_{A1} | = | empirical constant for equation (4.6) |
| β_{A2} | = | empirical constant for equation (4.7) |
| β_{A3} | = | empirical constant for equation (4.8) |
| β_{A4} | = | empirical constant for equation (4.9) |
| β_{A5} | = | empirical constant for equation (4.10) |
| β_{A6} | = | empirical constant for equation (4.11) |
| β_{B0} | = | empirical constant for equation (4.5) |
| β_{B1} | = | empirical constant for equation (4.6) |
| β_{B2} | = | empirical constant for equation (4.7) |
| β_{B3} | = | empirical constant for equation (4.8) |
| β_{B4} | = | empirical constant for equation (4.9) |
| β_{B5} | = | empirical constant for equation (4.10) |
| β_{B6} | = | empirical constant for equation (4.11) |
| $\varepsilon(x)$ | = | Horizontal strain |
| ρ | = | Maximum curvature |
| $\rho(x)$ | = | Curvature |
| ϕ | = | Friction angle |

CHAPTER I

INTRODUCTION

1.1 Rationale and background

Rock salt in the Maha Sarakham formation in the northeast of Thailand is separated into 2 basins: Sakon Nakhon basin and Khorat basin. Both basins contain three distinct salt units: Upper, Middle and Lower members. Sakon Nakhon basin in the north covers an area of approximately 17,000 square kilometers. Khorat basin in the south covers more than 30,000 square kilometers. From over 300 exploratory boreholes drilled primarily for oil and gas exploration, Suwanich (1978) estimates the geologic reserve of the three salt members from both basins as 18 MM tons. Vattanasak (2006) re-compiles the borehole data and proposes a preliminary design for salt solution mining caverns based on series of finite element analyses, and suggest that the inferred reserve of the Lower Salt member of the Khorat basin is about 20 billion tons. This estimation excludes the residential and national forest areas.

Salt and associated minerals in Khorat and Sakon Nakhon basins have become important resources for mineral exploitation and for use as host rock for product storage due to their wide spread and enormous amount. For over four decades, local people have extracted the salt by using an old fashion technique, called here as brine pumping method. A shallow borehole is drilled into the rock unit directly above the salt. Brine (saline groundwater) is pumped through the borehole and left evaporated on the ground surface. Relatively pure halite with slight amount of associated soluble mineral is then

obtained. This simple and low-cost method can however cause an environmental impact in forms of unpredictable ground subsidence, sinkhole and surface contamination.

The subsidence is caused by deforming or collapsing of large caverns at the interface between salt and the overburden formation. The locations of the induced surface subsidence and sinkholes are unpredictable due to the complexity of groundwater flow, infiltration of surface water and pumping locations and rates. Such severe surface subsidence and large sinkhole can cause property damage in and around the brine pumping industry. Geophysical method, have normally been employed to determine the size, depth and location of the underground caverns in the problem areas in an attempt to backfill the voids, and hence minimizing the damage of the engineering structures and farmland on surface. The geophysical investigation is however costly and time-consuming. This calls for a quick and low cost technique to determine the size, depth and location of the solution cavern underground.

1.2 Research Objectives

The objective of the proposed research is to develop a computer program to predict the location, depth, diameter and height of solution caverns created at the interface between rock salt and overlying rock mass. The effort involves simulation of surface subsidence induced by a variety of cavern configurations, laboratory testing to determine the shear strength of the overlying rock, formulation of mathematical relationship between the cavern configurations and surface profiles, development of computer software, and field verification.

1.3 Scope and Limitations

- 1) The study area is limited to Khorat and Sakon Nakhon basins.
- 2) FLAC is used to simulate the subsidence profiles.
- 3) The solution caverns are assumed to be half spherical and elliptical shapes.
- 4) Field investigation is carried out in the subsidence areas.
- 5) The resulted program is written in C language and Microsoft excel.
- 6) The cavern configurations are varied as follows; depth = 40 – 80 m, diameter = 20 – 100 m, and height = 5 – 20 m.

1.4 Research Methodology

Figure 1.1 depicts the research plan.

1.4.1 Literature Review

Literature review is carried out to improve an understanding of surface subsidence knowledge. The sources of information are from journals, technical reports, and conference papers. A summary of the literature review is given in the thesis.

1.4.2 FLAC Simulation

The profiles of surface subsidence are simulated using a finite difference program (FLAC) for the cavern diameters ranging from 10 m to 100 m, height from 5 m to 20 m and depths ranging from 40 m to 200 m.

1.4.3 Formulation of Mathematical Relationship

The results from the simulations are used to develop mathematic relationships between the surface subsidence and cavern geometry and depth. Such relationships are later used to develop computer program for predicting cavern configurations.

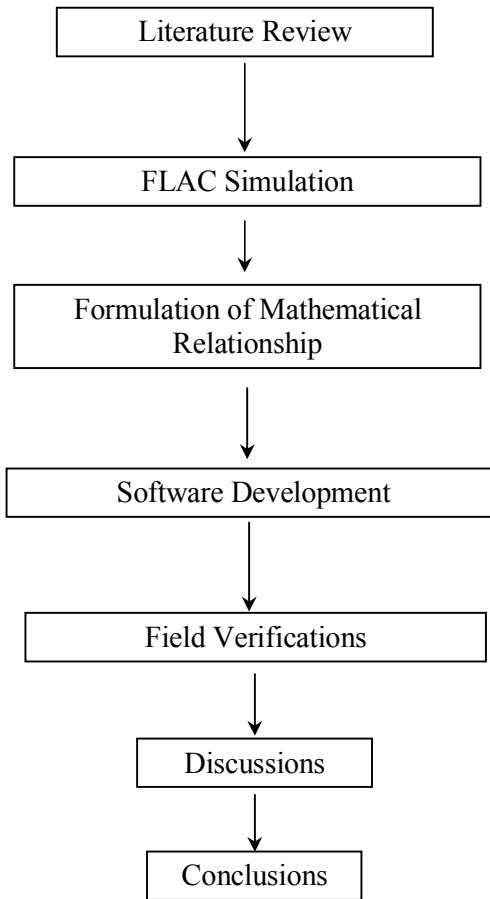


Figure 1.1 Research methodology.

1.4.4 Software Development

A computer program is developed in C language and Microsoft excel. The input data are the subsidence magnitudes, distributions, and slope profiles. The outputs are the cavern size, shape, depth, and location.

1.4.5 Field Verifications

Field investigations in relevant areas are carried out to verify the program output. Any discrepancy is examined. Correction and adjustment on the program parameters are made, if needed.

1.4.6 Thesis writing and presentation

All research activities, methods, and results are documented and compiled in the thesis.

1.5 Thesis Contents

Chapter I states the objectives, rationale, and methodology of the research. **Chapter II** summarizes results of the literature review on surface subsidence knowledge. **Chapter III** describes the profiles of surface subsidence are simulated using a finite difference program (FLAC) and profile function. **Chapter IV** describes develop mathematic relationships, software development and field verifications. Conclusions and recommendations for future research needs are given in **Chapter V**.

CHAPTER II

LITERATURE REVIEW

2.1 Introduction

Topics relevant to this research are reviewed to improve an understanding of surface subsidence knowledge. These include rock salt in the northeast of Thailand, calculation of surface subsidence profile, FLAC program, and SALT_Subsid program. Results from the preliminary review are summarized as follows.

2.2 Rock salt in northeast region of Thailand

Rock salt formation in Thailand is located in the Khorat plateau as shown in Figure 2.1. The Khorat plateau covers 150,000 square kilometers, from 14° to 19° northern latitude and 101° to 106° eastern longitude. The northern and eastern edges of the plateau lie close to Laos and the southern one close to Cambodia (Utha-aroon, 1993).

Rock salt is separated into 2 basins: Sakon Nakhon Basin and Khorat Basin. The Sakon Nakhon Basin in the north has an area about 17,000 square kilometers. It covers the area of Nong Khai, Udon Thani, Sakon Nakhon, Nakhon Phanom, and Mukdahan provinces and extends to some part of Laos. The Khorat Basin is in the south, which has about 33,000 square kilometers. The basin covers the area of Nakhon Ratchasima, Chaiyaphum, Khon Kaen, Maha Sarakham, Roi Et, Kalasin, Yasothon, Ubon Ratchathani provinces and the north of Buriram, Surin, and Sisaket provinces (Suwanich, 1986).

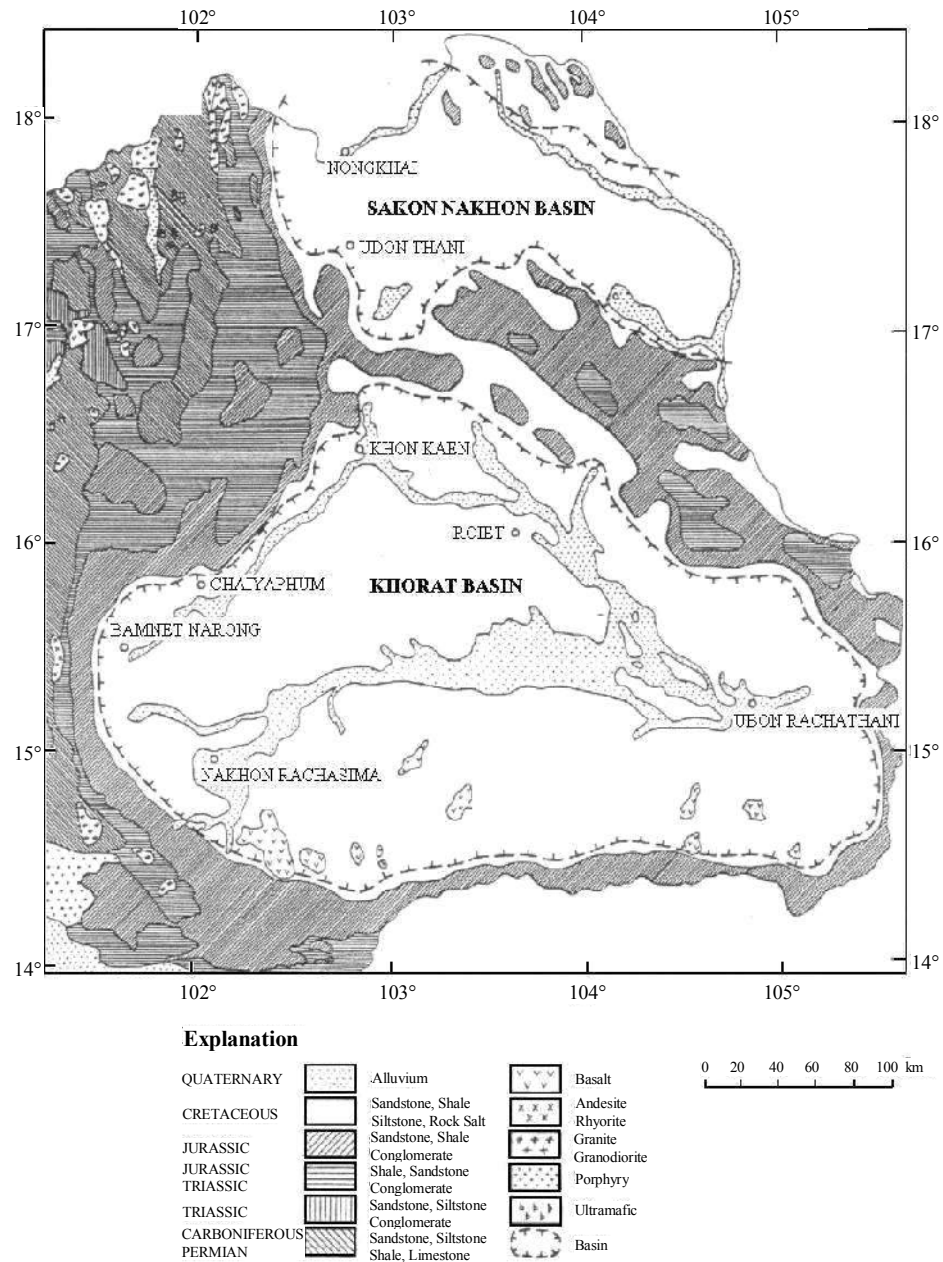


Figure 2.1 Sakon Nakhon and Khorat Basins containing rock salt in the northeast of Thailand (modified from Rattanajurak, 1990 and Utha-aroon, 1993 adapted from Geological Map of Thailand, scale 1:2,500,000).

The Department of Mineral Resources had drilled 194 drilled holes between 1976 and 1977 for the exploration of potash (Japakasetr, 1985; Japakasetr and Workman, 1981; Sattayarak, 1983, 1985; Japakasetr, 1992; Japakasetr and Suwanich, 1982). Some holes were drilled through rock salt layers to the Khok Kruat Formation (Yumuang et al., 1986; Supajanya et al., 1992; Utha-aroon, 1993; Warren, 1999). The sequences of rock layers from the bottom of this formation up to the top of the Maha Sarakham Formation are as follows.

- 1) Red bed sandstone or dense greenish gray siltstone sometime intercalated with reddish-brown shale.
- 2) Basal anhydrite with white to gray color, dense, lies beneath the lower rock salt and lies on the underlying Khok Kruat Formation.
- 3) Lower rock salt, the thickest and cleanest rock salt layer, except in the lower part which contains organic substance. The thickness exceeds 400 meters in some areas and formed salt domes with the thickness up to 1,000 meters, with the average thickness of 134 meters.
- 4) Potash, 3 types were found; carnallite ($\text{KCl} \cdot \text{MgCl}_2 \cdot 6\text{H}_2\text{O}$) with orange, red and pink color, sylvinite (KCl) rarely found, white and pale orange color, an alteration of carnallite around salt domes, and techydrite ($\text{CaCl}_2 \cdot 2\text{MgCl}_2 \cdot 12\text{H}_2\text{O}$) often found and mixed with carnallite, orange to yellow color caused by magnesium, the dissolved mineral occurred in place.
- 5) Rock salt, thin layers with average thickness of 3 meters, red, orange, brown, gray and clear white colors.
- 6) Lower clastic, clay and shale, relatively pale reddish-brown color and mixed with salt ore and carnallite ore.

7) Middle salt, argillaceous salt, pale brown to smoky color, thicker than the upper salt layer with average thickness of 70 meters, carnallite and sylvite may be found at the bottom part.

8) Middle clastic, clay and shale, relatively pale reddish brown color and intercalated with white gypsum.

9) Upper salt, dirty, mixed with carbon sediment, pale brown to smoky color or orange color when mixed with clay and 3 to 65 meters thick.

10) Upper anhydrite, thin layer and white to gray color.

11) Clay and claystone, reddish brown color, occurrence of siltstone and sandstone in some places, and

12) Upper sediment, brownish gray clay and soil in the upper part, and sandy soil and clay mixed with brown, pink and orange sandy soil in the lower part.

Cross-sections from seismic survey across the Khorat-Ubon and Udon-Sakon Nakhon Basins (Sattayarak and Polachan, 1990) reveal that rock salt can be categorized into 3 types according to their appearances namely, rock salt beds, rock salt fold and salt domes. The Maha Sarakham and Phu Tok Formations fold in harmony with the Khorat megasequence. A part of the cross section through the Khorat Basin is illustrated in Figure 2.2.

2.3 Site conditions

Figure 2.3 also shows the areas where the brine pumping have been practices. Depths of the shallowest salt in those areas vary from 40 m to 200 m. It belongs to the Middle or Lower member, depending on locations. Most of the brine pumping practices are however in the areas where the topography is flat, groundwater table is

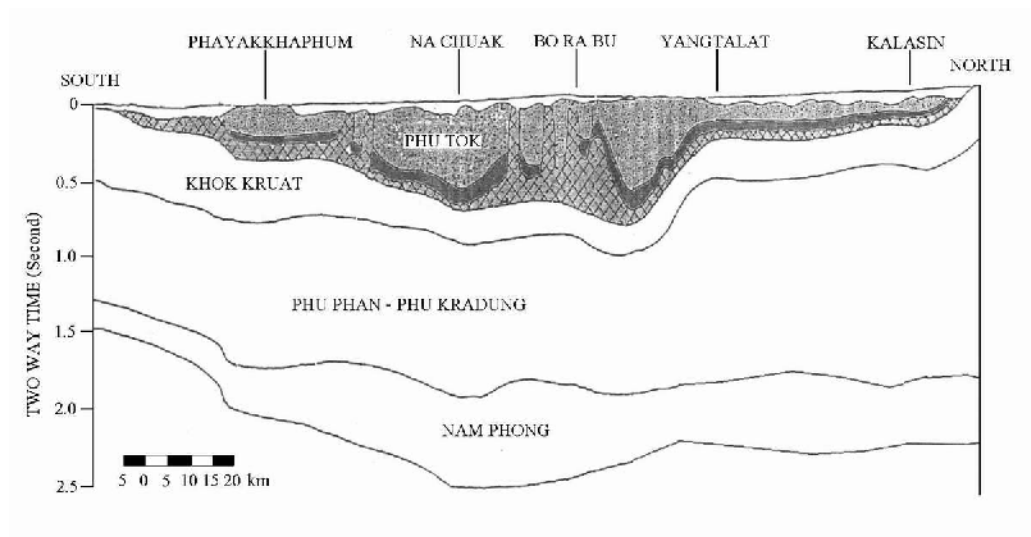


Figure 2.2 Cross-section showing rock salt in the Khorat Basin (from Sattayarak, 1985).

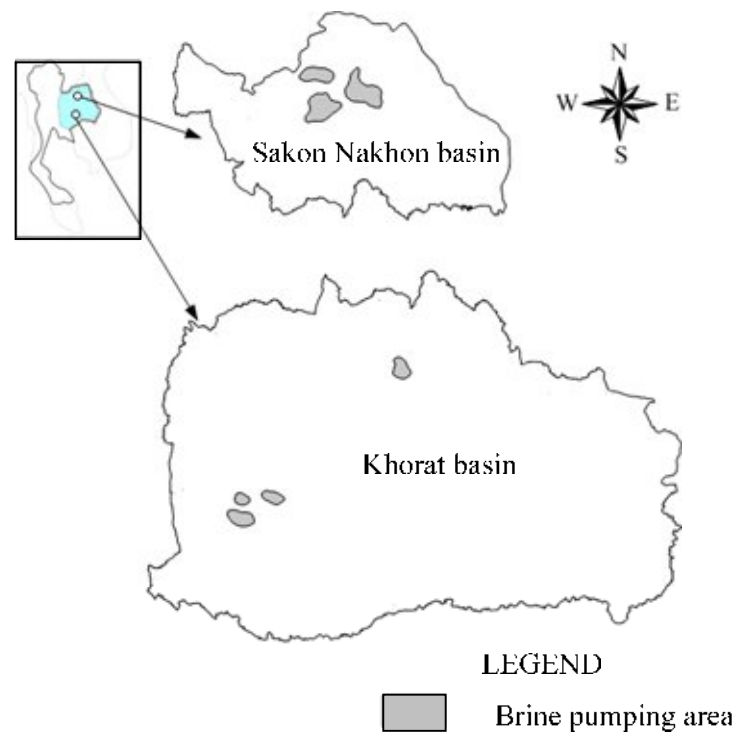


Figure 2.3 Brine pumping area in Khorat and Sakon Nakhon salt basins.

near the surface, and the salt depth is less than 50 m in the Sakon Nakhon basin, and about 100 m in the Khorat basin (Jenkunawat, 2005; Wannakao et al., 2005). Based on field investigation, Jenkunawat (2007) states that the surface subsidence normally occurs in the areas where depth of the shallowest salt is less than 50 m. The overburden consists mainly of mudstone siltstone and sandstone of the Middle Clastic, and claystone and mudstone of the Lower Clastic, with fractures typically dipping less than 30 degrees, and rarely at 70 degrees (Crosby, 2007). The members are characterized by abundant halite and anhydrite-filled fractures and bands with typical thickness of 2 cm to 5 cm.

Direct shear tests performed in this research yield the cohesion and friction angle of 0.30 MPa and 27° for the smooth saw-cut surfaces prepared from the Middle Clastic siltstone. More mechanical properties for these clastic members are summarized by Wannakao et al. (2004) and Crosby (2007).

Wannakao and Walsri (2007) state that one third of the northeast is generally underlain by sedimentary rocks of Maha Sarakham Formation, sequences of rock salt and clastic rocks. The deposits are divided into the Khorat and Sakon Nakhon basins. Salt productions from brine groundwater are common in both basins. A brine groundwater well is 4 in diameter with 2 in air pumping line at about 60-100 meters depth. The brine is pumped to salt storage bin, then conveyed to salt paddy field for solar evaporation. There are many surface subsidence reported in salt production area in Ban Non Sabaeng, Sakon Nakhon province

Jenkunawat (2007) study occurrence of salt cavities induced by brine pumping. The main purpose is to delineate disaster area and monitor land subsidence. Drill holes were totally 12 with depth ranged 100-200 m. A number of holes were constructed as

monitoring wells to observe circulation patterns of the brine by cased them with PVC pipes. Drilling results showed claystone at top, salt dome located under the salt production area at depth of 40-50 m. Rock salt was located at depth 40-200 m. Anhydrite and gypsum were observed in holes around the salt dome. Sinkholes are circular in shape, with diameter of 50-100 m. Land usually starts subsiding at pumping well and moves in a series of subsidence which can be traced in a line. They occur in only on a salt dome, where there are fractures, brine zone and dissolution of salt. Areas out of the salt dome are not under risk of salt subsidence.

2.4 Calculation of surface subsidence

2.4.1 Theory and criterion

Singh (1992) states that subsidence is an inevitable consequence of underground mining – it may be small and localized or extend over large areas, it may be immediate or delayed for many years. During recent years, with the expansion of urbanization and increased concern for the environment, it is no longer possible to ignore its aftermath.

The major objectives of subsidence engineering are 1) Prediction of ground movement, 2) Determining the effects of such movements on structures and renewable resource and 3) Minimizing damage due to subsidence.

Whenever a cavity is created underground, due to the mining of minerals or for any other reason, the stress field in the surrounding strata is disturbed. These stress changes produce deformations and displacements of the strata, the extent of which depends on the magnitude of the stresses and the cavity dimensions. With time, supporting structures deteriorate and the cavity enlarges, resulting in instability.

This induces the superjacent strata to move into the void. Gradually, these movements work up to the surface, manifesting themselves as a depression. This is commonly referred to as subsidence. Thus mine subsidence may be defined as ground movements that occur due to the collapse of overlying strata into mine voids. Surface subsidence generally entails both vertical and lateral movements.

Surface subsidence manifests itself in three major ways: 1) cracks, fissures, or step fractures, 2) pits or sinkholes and 3) troughs or saga. Surface fractures may be in the form of open cracks, stepped slips, or cave - in pits and reflect tension or shear stresses in the ground surface. Subsidence consists of five major components, which influence damage to surface structures and renewable resources are vertical displacement, horizontal displacement, slope, vertical strain, and vertical curvature.

Calculation by profile function;

Subsidence:

$$S(x) = \frac{1}{2} S_{\max} \left[1 - \tanh\left(\frac{cx}{B}\right) \right] \quad (2.1)$$

Slope:

$$G(x) = S'(x) = -\frac{1}{2} S_{\max} \frac{c}{B} \operatorname{sech}^2\left(\frac{cx}{B}\right) \quad (2.2)$$

Curvature:

$$\rho(x) = S''(x) = S_{\max} \frac{c^2}{B^2} \left[\operatorname{sech}^2\left(\frac{cx}{B}\right) \tanh\left(\frac{cx}{B}\right) \right] \quad (2.3)$$

Horizontal displacement:

$$u(x) = -\frac{1}{2} S_{\max} \frac{bc}{B} \operatorname{sech}^2\left(\frac{cx}{B}\right) \quad (2.4)$$

Horizontal strain:

$$\varepsilon(x) = S_{\max} \frac{bc^2}{B^2} \left[\operatorname{sech}^2\left(\frac{cx}{B}\right) \tanh\left(\frac{cx}{B}\right) \right] \quad (2.5)$$

where S_{\max} is the maximum subsidence, D is depth of cavern, γ is angle of draw, x is horizontal distance, c is arbitrary constant, b is constant, and B is maximum radius of cavern area.

2.4.2 Calculation with SALT_SUBSID program

SALT_SUBSID code developed by RE/SPEC Inc. (Nieland, 1991) has been used to predict the three-dimensional surface subsidence for predicting configurations of solution cavern on top of salt bed. SALT_SUBSID is designed to calculate the subsidence profile induced by dry mining (underground openings) and solution mining (brine caverns). The key parameters used in SALT_SUBSID including Y_{ss} , Y_o , β and N have been calibrated using the subsidence results computed by the finite element analysis. This makes the predicted subsidence profile over the cavern field more site-specific. Definition of these parameters is described in details by Nieland (1991).

$$Z(x,y,t) = Z_u(x,y).G(t) \quad (2.6)$$

$$G(t) = Y_{ss}.t + Y_o[1 - \exp(-\beta E^N t)], \text{ and} \quad (2.7)$$

$$G(t) = 1; \text{ if } Y_{ss} \cdot t + Y_o[1 - \exp(-\beta E^N t)] > 1 \quad (2.8)$$

where Y_{ss} , Y_o , β , N are model parameters, t is time since excavation, E is extraction ratio of the mine, and Z_u is ultimate surface displacement at any location.

The condition that $G(t) = 1$ is applied when a cavity is completely closed. The parameter Y_{ss} represents the steady-state closure rate and Y_o represents the ultimate transient closure. The parameters β and N are empirical constants used to model the transient closure rate. In the case of dry mining, the parameter Y_{ss} is set to zero.

2.4.3 FLAC program

FLAC (Itasca, 1992a, 1992b) is a two-dimensional explicit finite difference program for engineering mechanics computation. This program simulates the behavior of structures built of soil, rock or other materials that may undergo plastic flow when their yield limits are reached. Materials are represented by elements, or zones, which form a grid that is adjusted by the user to fit the shape of the object to be modeled. Each element behaves according to a prescribed linear or nonlinear stress/strain law in response to the applied forces or boundary restraints. The material can yield and flow and the grid can deform (in large-strain mode) and move with the material that is represented. The explicit, Lagrangian calculation scheme and the mixed-discretization zoning technique used in FLAC ensure that plastic collapse and flow are modeled very accurately. Because no matrices are formed, large two-dimensional calculations can be made without excessive memory requirements. The drawbacks of the explicit formulation (i.e., small timestep limitation and the question of required damping) are overcome to some extent by automatic inertia scaling and automatic damping that do not influence the mode of failure.

Though FLAC was originally developed for geotechnical and mining engineers, the program offers a wide range of capabilities to solve complex problems in mechanics. Several built-in constitutive models are available that permit the simulation of highly nonlinear, irreversible response representative of geologic, or similar, materials.

CHAPTER III

NUMERICAL SIMULATIONS

3.1 Introduction

This chapter describes the finite difference analyses with FLAC code (Itasca, 1992) to study the surface subsidence profile correlated with the overburden mechanical properties, cavern depth and cavern height. The model simulations and results are presented. The calculations of surface subsidence using are also made.

3.2 Finite Difference Simulations

Finite difference analyses are performed to correlate the surface components with the cavern depth and diameter. The FLAC code is used here to simulate the subsidence magnitude, surface slope, cavern roof deformation and radius of influence on the surface. The variables include cavern diameter, cavern depth, and overburden mechanical properties. To cover the entire range of the cavern ground conditions, over 400 finite difference meshes have been constructed to represent cavern diameters (w) varying from 20 m to 100 m with an interval of 10 m, and the cavern depths (d) from 40, 60 to 80 m. Figure 3.1 gives an example of the computer model. The analysis is made in axial symmetry and under a hydrostatic stress field. The cavern is assumed to be half-oval shaped, and is under hydrostatic pressure of saturated brine. The groundwater table is assumed to be at the ground surface. The cavern is assumed under drained condition. The overburden is represented by a single

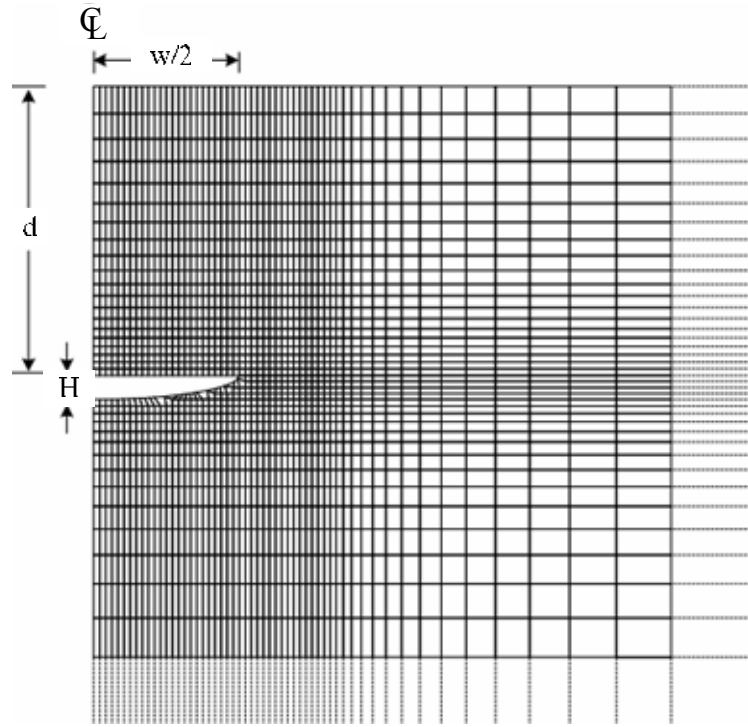


Figure 3.1 Example of finite difference mesh used in FLAC simulation. Analysis is made in axial symmetry. $H = 5$ m, $d = 60$ m, $w = 60$ m, $B = 172$ m, $E_m = 40$ MPa and $\phi = 20^\circ$.

unit of elastic rock with deformation moduli varying from 20, 40, 60, to 80 MPa, and internal friction angles from 20, 40, to 60 degrees. The cohesion is assumed to be zero in all cases. This assumption is supported by the experimental results of Barton (1974) and Grøneng *et al.* (2009) who found that the cohesion of rock mass comprising claystone, mudstone and siltstone were zero or negligible. The overburden is assumed to behave as an elastic – plastic material. The overburden behaves as linear elastic material when the shear stress is less than the shear strength defined by the friction angle. When the shear stress exceeds the strength the overburden behaves as perfectly plastic material. The constitutive equations and derivation of yield and potential functions for this elastic – plastic material are given in detail by Itasca (1992). The mechanical properties of the elastic rock used here are within the range of those compiled by Thiel and Zabuski (1993).

3.3 Results

The simulation results are shown in terms of the subsidence magnitude at the ground surface and distribution of shear stresses. The variables used in FLAC simulations as shown in Table 3.1. Figures 3.2 through 3.6 shows the examples of subsidence results for 5 depth levels. Each depth varies the cavern diameters and height. The results indicate that the subsidence profile can be shown in form of a hyperbolic curve. The cavern diameter and height are correlated with the maximum surface subsidence and subsidence area. The ground subsidence profile varies with the cavern depth and diameter. The results show that the maximum subsidence decreases with increasing the cavern depth, and increases with increasing the cavern diameter.

Table 3.1 Variables used in FLAC simulations. The deformation moduli (E_m) vary from 20, 40, 60 to 80 MPa and friction angle (ϕ) vary from 20°, 40° to 60°.

| Cavern Depth (d) | Cavern Height (H) | Cavern Diameter (w) | d/w Ratio |
|---------------------|----------------------|------------------------|-----------|
| 40 | 5 | 20 | 2.00 |
| | | 30 | 1.33 |
| | | 40 | 1.00 |
| | | 50 | 0.80 |
| | | 60 | 0.66 |
| | | 70 | 0.57 |
| | | 80 | 0.50 |
| 60 | 5 | 20 | 3.00 |
| | | 30 | 2.00 |
| | | 40 | 1.50 |
| | | 50 | 1.20 |
| | | 60 | 1.00 |
| | | 70 | 0.86 |
| | | 80 | 0.75 |
| | | 90 | 0.67 |
| | | 100 | 0.60 |
| 80 | 5 | 20 | 4.00 |
| | | 30 | 2.67 |
| | | 40 | 2.00 |
| | | 50 | 1.60 |
| | | 60 | 1.33 |
| | | 70 | 1.14 |
| | | 80 | 1.00 |
| | | 90 | 0.89 |
| | | 100 | 0.80 |

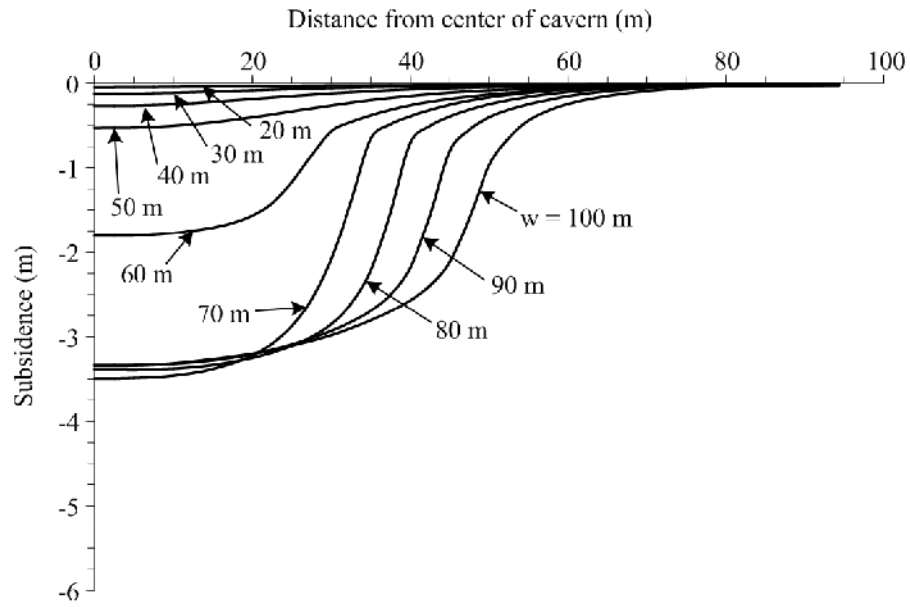


Figure 3.2 The maximum subsidence (S_{\max}) from FLAC simulations. $d = 40$ m and $H = 5$ m.

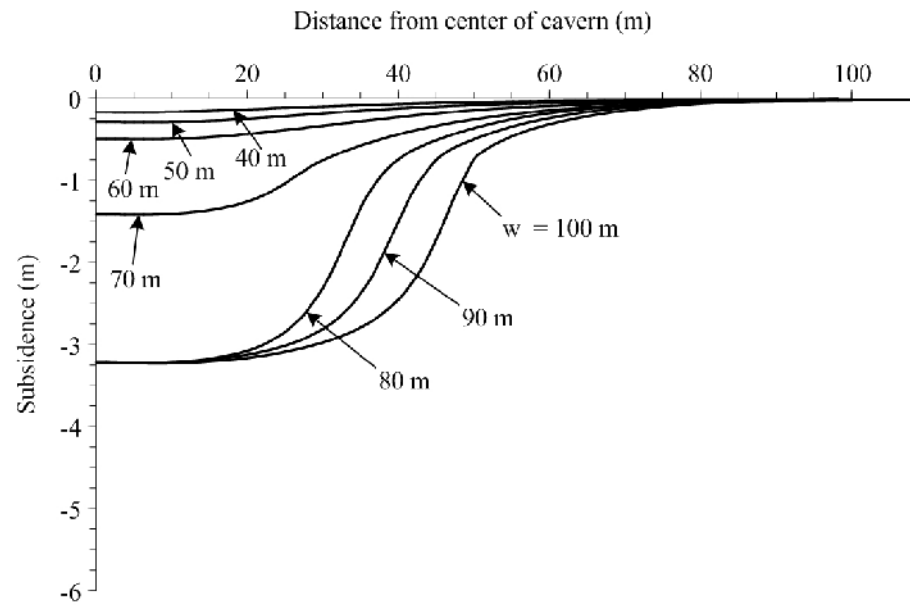


Figure 3.3 The maximum subsidence (S_{\max}) from FLAC simulations. $d = 50$ m and $H = 5$ m.

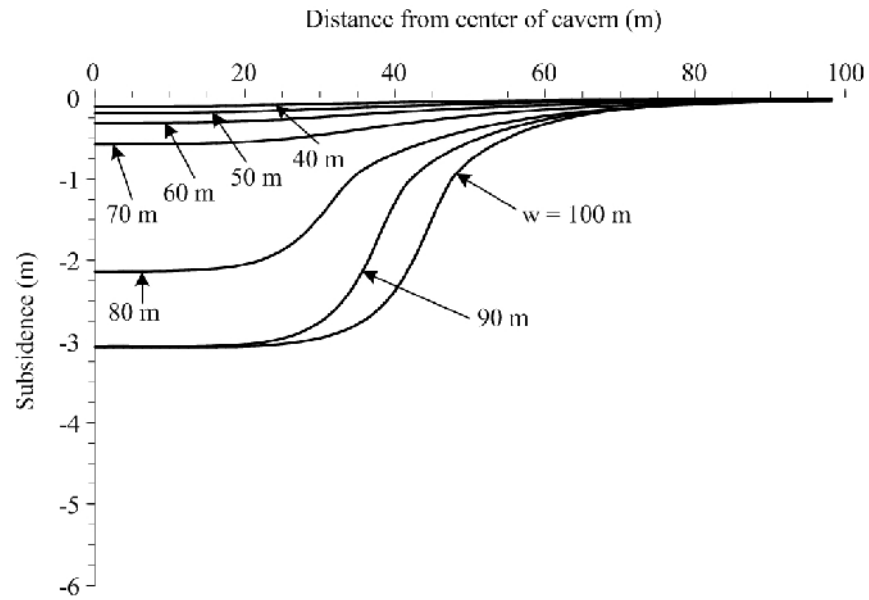


Figure 3.4 The maximum subsidence (S_{\max}) from FLAC simulations. $d = 60$ m and $H = 5$ m.

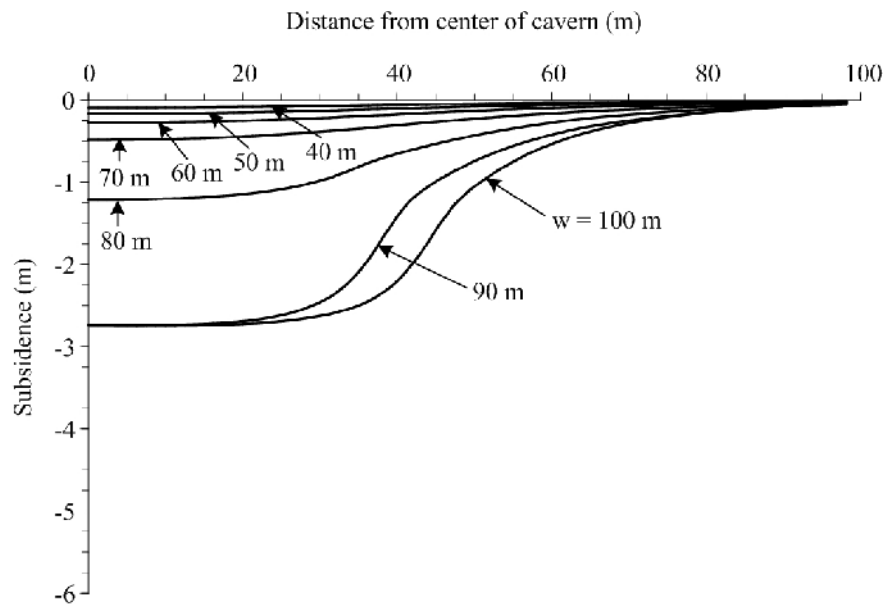


Figure 3.5 The maximum subsidence (S_{\max}) from FLAC simulations. $d = 70$ m and $H = 5$ m.

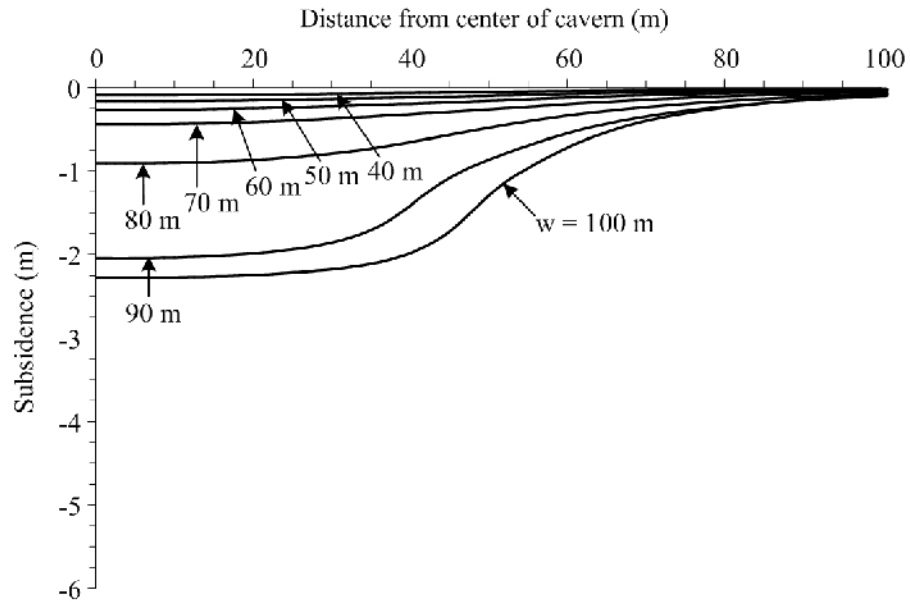


Figure 3.6 The maximum subsidence (S_{max}) from FLAC simulations. $d = 80$ m and $H = 5$ m.

When the solution cavern diameter reaches the critical point, the subsidence profile is not hyperbolic. This situation is called critical cavern diameter (w_{cri}). The w_{cri} can be correlated with the maximum subsidence and maximum slope of the ground surface. These empirical relations are used to predict the cavern depth (d), cavern diameter (w), roof deformation (R_s) and radius of influence ($B/2$). They are presented in the next chapter.

3.4 Profile function

Singh (1992) states that subsidence is an inevitable consequence of underground mining – it may be small and localized or extend over large areas, it may be immediate or delayed for many years. During recent years, with the expansion of urbanization and increased concern for the environment, it is no longer possible to ignore its aftermath.

The major objectives of subsidence engineering are (1) prediction of ground movement, (2) determining the effects of such movements on structures and renewable resource and (3) minimizing damage due to subsidence.

Whenever a cavity is created underground, due to the mining of minerals or for any other reason, the stress field in the surrounding strata is disturbed. These stress changes produce deformations and displacements of the strata, the extent of which depends on the magnitude of the stresses and the cavity dimensions. With time, supporting structures deteriorate and the cavity enlarges, resulting in instability. This induces the superjacent strata to move into the void. Gradually, these movements work up to the surface, manifesting themselves as a depression. This is commonly referred to as subsidence. Thus mine subsidence may be defined as ground movements that occur due to the collapse of overlying strata into mine voids. Surface subsidence generally entails both vertical and lateral movements.

Subsidence consists of five major components, which influence damage to surface structures and renewable resources are vertical displacement, horizontal displacement, slope, vertical strain and vertical curvature. They can be calculated as (Singh, 1992):

Vertical displacement:

$$S(x) = \frac{1}{2} S_{\max} \left[1 - \tanh\left(\frac{cx}{B}\right) \right] \quad (3.1)$$

Slope:

$$G(x) = S'(x) = -\frac{1}{2} S_{\max} \frac{c}{B} \operatorname{sech}^2\left(\frac{cx}{B}\right) \quad (3.2)$$

Curvature:

$$\rho(x) = S''(x) = S_{\max} \frac{c^2}{B^2} \left[\operatorname{sech}^2\left(\frac{cx}{B}\right) \tanh\left(\frac{cx}{B}\right) \right] \quad (3.3)$$

Horizontal displacement:

$$u(x) = -\frac{1}{2} S_{\max} \frac{bc}{B} \operatorname{sech}^2\left(\frac{cx}{B}\right) \quad (3.4)$$

Horizontal strain:

$$\varepsilon(x) = S_{\max} \frac{bc^2}{B^2} \left[\operatorname{sech}^2\left(\frac{cx}{B}\right) \tanh\left(\frac{cx}{B}\right) \right] \quad (3.5)$$

where S_{\max} is the maximum subsidence, D is depth of cavern, γ is angle of draw, x is horizontal distance, c is arbitrary constant, b is constant and B is maximum radius of cavern area.

The computer simulations are compared with those calculated by Singh's hyperbolic function for some cases in Figures 3.7 through 3.12. FLAC simulation gives the subsidence magnitudes about 10% difference from the hyperbolic function. The maximum surface slopes calculated from both methods are similar.

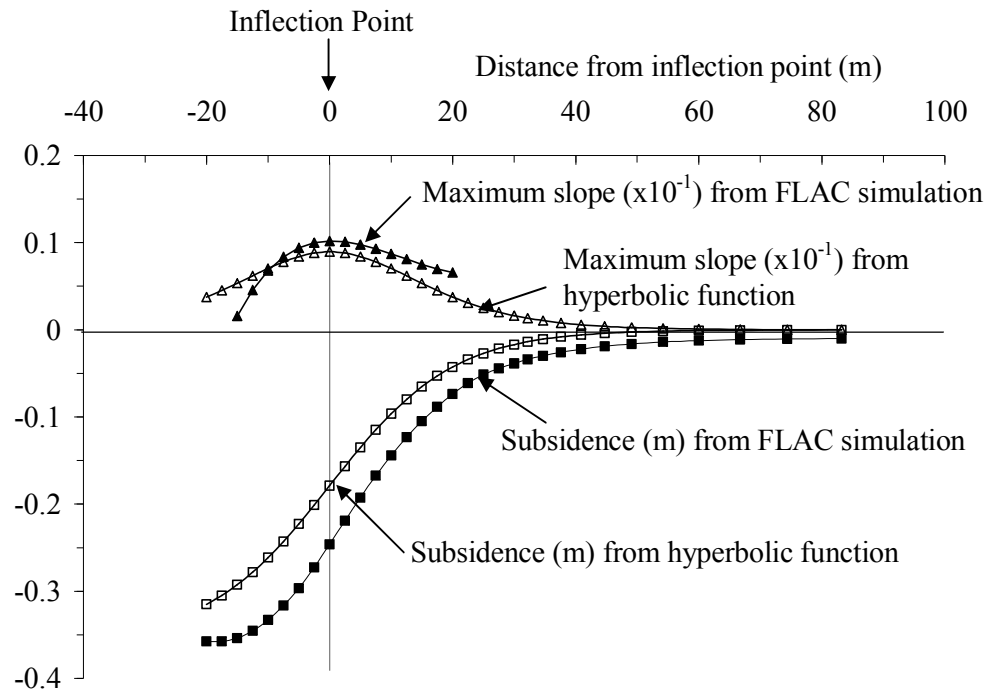


Figure 3.7 FLAC simulations compared with hyperbolic function calculations for $\phi = 20^\circ$, $E_m = 20$ MPa, $d = 40$ m and $w = 40$ m.

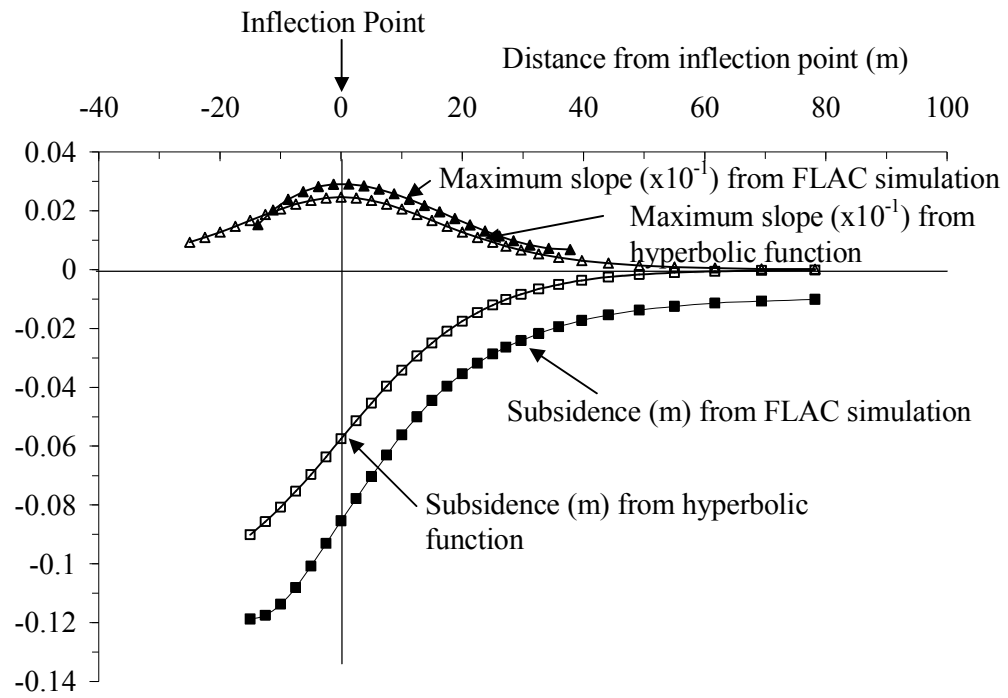


Figure 3.8 FLAC simulations compared with hyperbolic function calculations for

$\phi = 20^\circ$, $E_m = 40$ MPa, $d = 40$ m and $w = 40$ m.

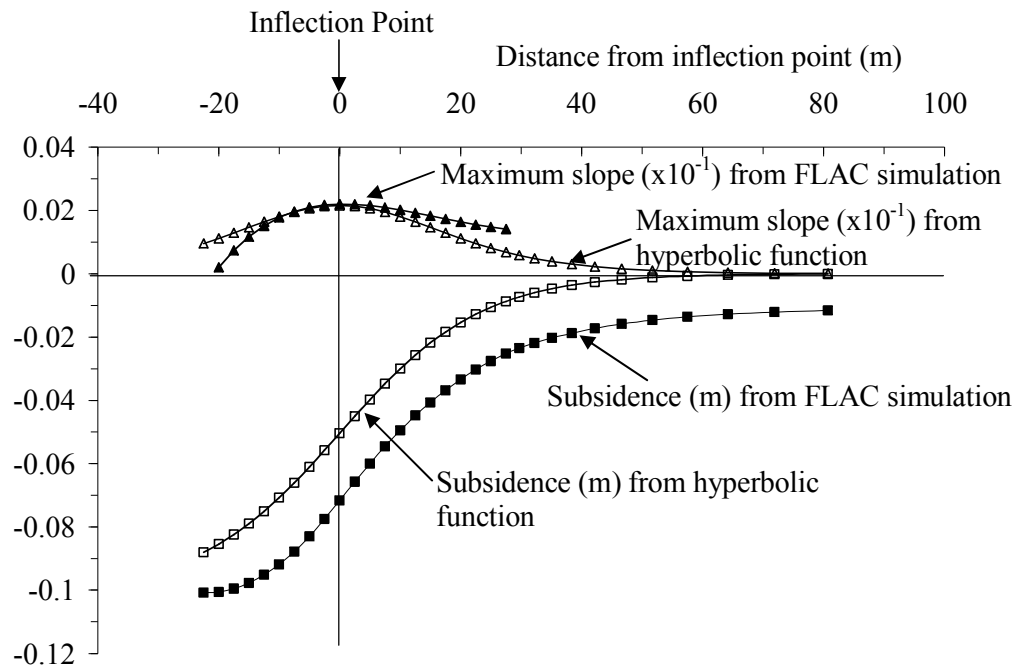


Figure 3.9 FLAC simulations compared with hyperbolic function calculations for $\phi = 20^\circ$, $E_m = 60$ MPa, $d = 40$ m and $w = 40$ m.

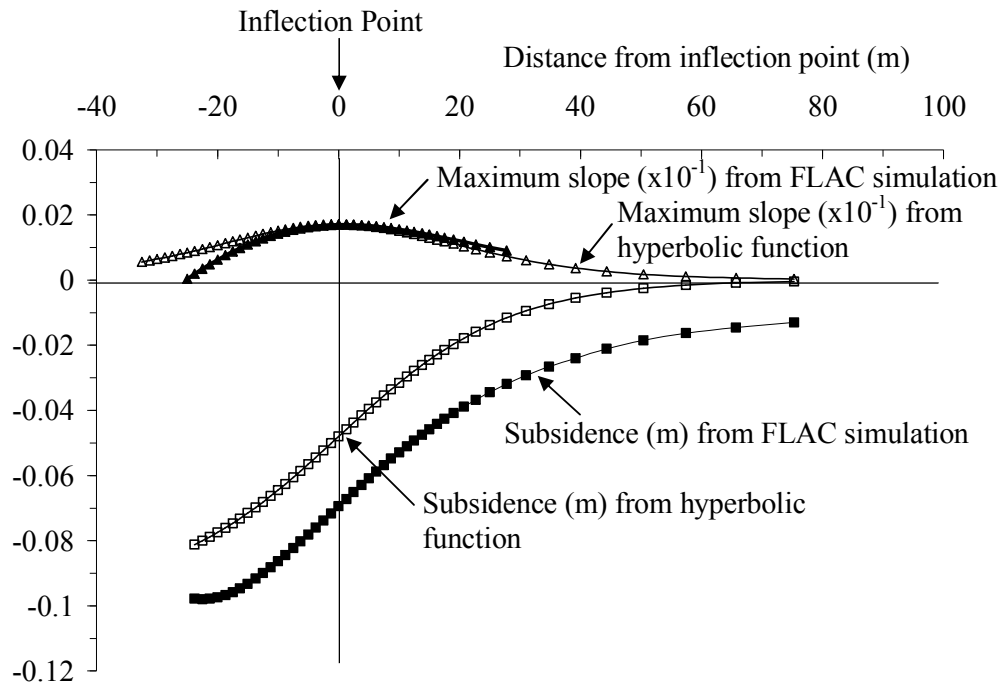


Figure 3.10 FLAC simulations compared with hyperbolic function calculations for

$\phi = 20^\circ$, $E_m = 20$ MPa, $d = 60$ m and $w = 40$ m.

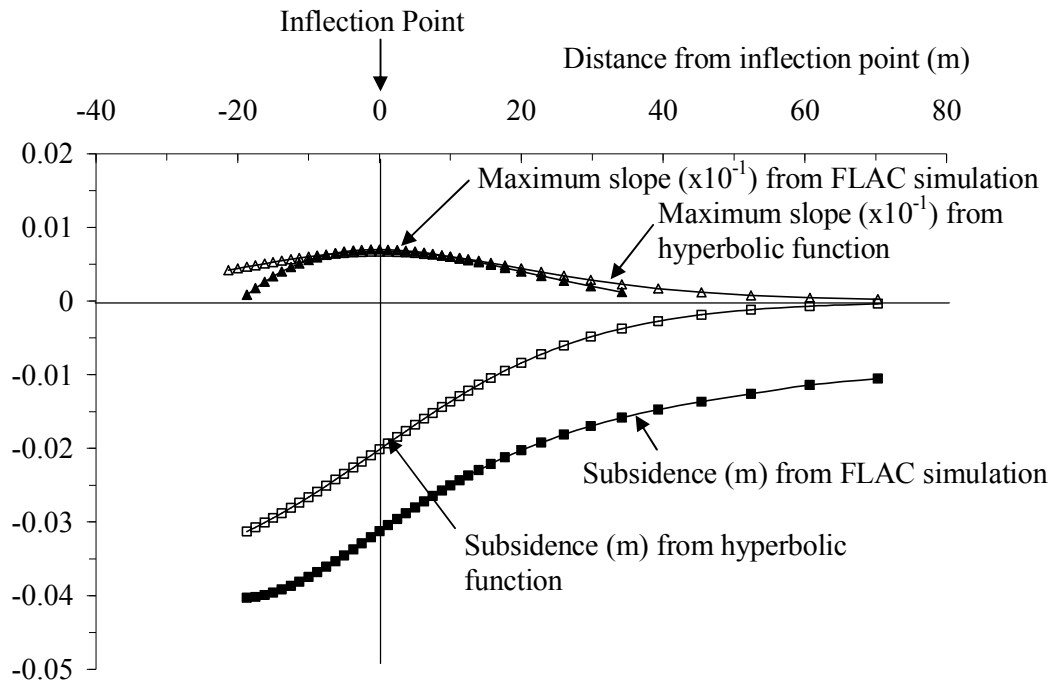


Figure 3.11 FLAC simulations compared with hyperbolic function calculations for

$\phi = 20^\circ$, $E_m = 40$ MPa, $d = 60$ m and $w = 40$ m.

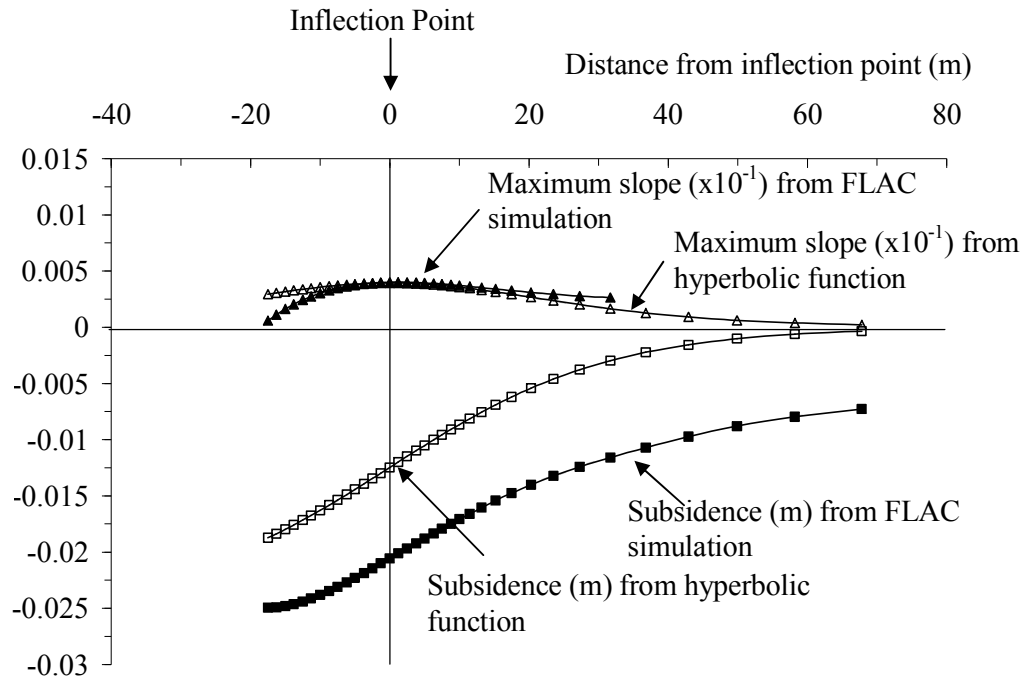


Figure 3.12 FLAC simulations compared with hyperbolic function calculations for

$\phi = 20^\circ$, $E_m = 60$ MPa, $d = 60$ m and $w = 40$ m.

CHAPTER IV

MATHEMATICAL RELATIONSHIPS

4.1 Introduction

This chapter describes a method to determine the subsidence profile from the ground survey data. A statistical analysis method is used to correlate between the maximum subsidence magnitude, maximum slope, curvature, cavern depth and cavern diameter. The empirical equations developments are developed for the surface subsidence under sub-critical and critical conditions.

4.2 Statistical analysis of the ground survey data

A statistical method is developed to determine the maximum subsidence magnitude, maximum slope profile, curvature of the ground surface, and the cavern location. The regression is performed on the ground survey data obtained from subsiding areas. It is assumed here that the cavern model is a half-oval shaped with the maximum diameter, w , located at the contact between the salt and the overburden. The ground surface, overburden and salt are horizontal. Figure 4.1 identifies the variables used in this study. The radius of influence ($B/2$) represents the radius of the subsiding area where the vertical downward movement of the ground equals 1 cm or greater.

The survey data referred to here are the vertical displacements of the ground surface (z) measured at various points with respect a global x-y coordinate (Figure 4.2). A hyperbolic function modified from Singh (1992) is proposed to govern the

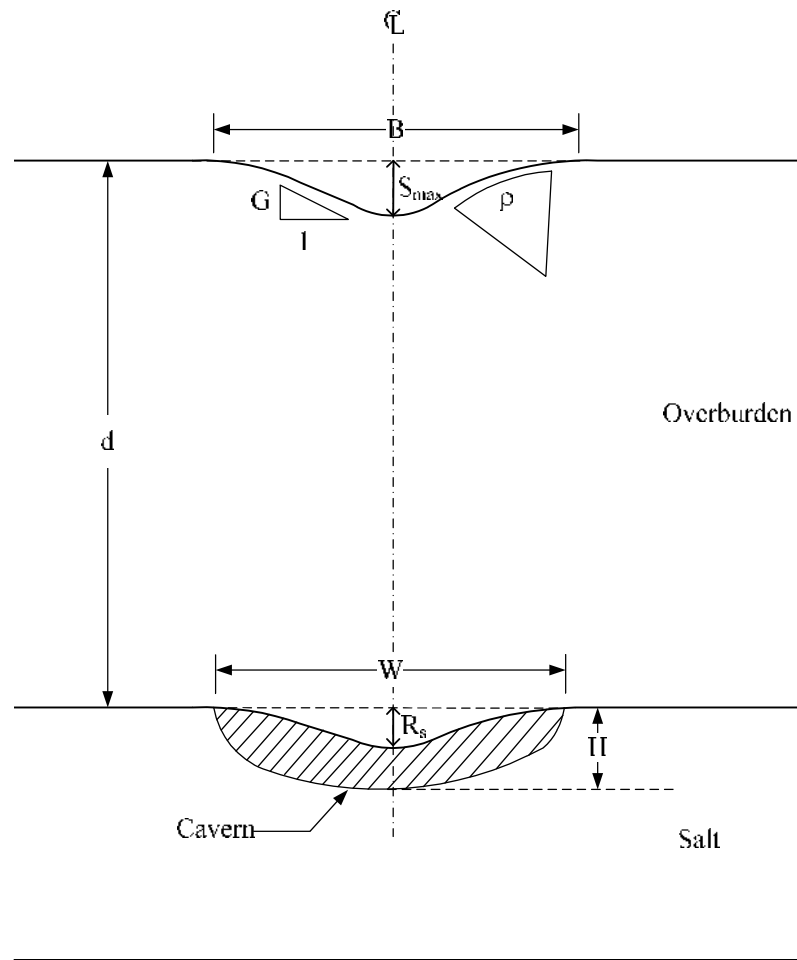


Figure 4.1 Variables used in this study.

characteristics of surface subsidence profile. It expresses the subsidence function, $S(r_i)$ (subsidence magnitude at point 'i', where i varied from 1 to the total number of measurements, n) as:

$$S(r_i) = a_0 \tanh(10a_1r_i - a_2) + a_3 \quad (i = 1, 2, 3, \dots, n) \quad (4.1)$$

$$\text{when } r_i = \sqrt{(x_i - a_4)^2 + (y_i - a_5)^2} \quad (4.2)$$

where r_i = distance from data point 'i' to the center of the group of data,

x_i, y_i = coordinates of subsidence measured at point 'i'

a_0, a_1, a_2, a_3, a_4 and a_5 are constants related to the subsidence components and coordinates of the maximum subsidence location, which can be defined as:

a_0 = half of the maximum subsidence (S_{\max}),

a_1 = scaling factor,

a_2 = planar offset,

a_3 = vertical offset,

$a_4 = \sum x_i/n$, and

$a_5 = \sum y_i/n$.

The above equation is modified from the hyperbolic function of Singh (1992) to allow a statistical analysis of field measurement data, and subsequently provides a smooth three-dimensional profile of surface subsidence for further analysis.

Similarly, the maximum slope (G) of the surface subsidence induced at the inflection point can be determined as:

$$G = S'(r_i) = 10a_0 \times a_1 \operatorname{sech}^2(10a_1r_i - a_2) \quad (4.3)$$

The maximum curvature (ρ) of the ground surface is calculated as:

$$\rho = S''(r_i) = -200a_0a_1^2 \operatorname{sech}^2(10a_1r_i - a_2) \times \tanh(10a_1r_i - a_2) \quad (4.4)$$

Regression analysis of the survey data using equation (4.1) will provide the three subsidence components and cavern location. These components are correlated with the cavern depth, cavern diameter, roof deformation and radius of influence. The regression also provides a smooth profile of the subsidence in three-dimension, as shown in Figure 4.2. Accuracy of the results depends on the number of the field measurements.

A computer program is developed to calculate the cavern depth, cavern diameter, roof deformation and radius of influence on the ground surface. The program for regression is written in C language. The source code is given in Appendix A. The program for calculating of the cavern depth, diameter, roof deformation and radius of influence are written in Microsoft Excel.

It is recognized that several theoretical models and governing equations have been developed to predict the subsiding characteristics of the ground surface induced by underground openings (e.g., Nieland, 1991; Shu and Bhattacharyya, 1993; Cui et al., 2000; Asadi et al., 2005). Singh (1992) also proposes several profile functions to represent the subsidence characteristics above mine openings. Singh's hyperbolic function is used here because it is simple and can provide results close to those obtained from numerical simulations (it mentions in Chapter 3).

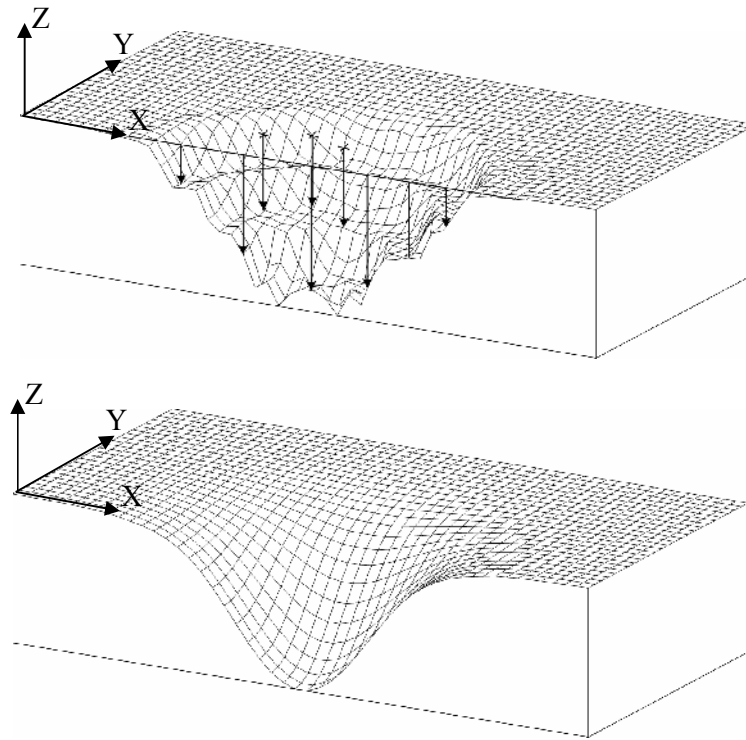


Figure 4.2 Regression of ground survey data (top) to obtain a representative hyperbolic profile of ground surface (bottom). Vertical scale is greatly exaggerated.

4.3 Empirical equations

After several trials the critical cavern diameters (the maximum diameter before failure occurs) can be determined along with their corresponding cavern depths, roof deformations, and mechanical properties of the overburden. This therefore represents the critical condition as defined by Singh (1992).

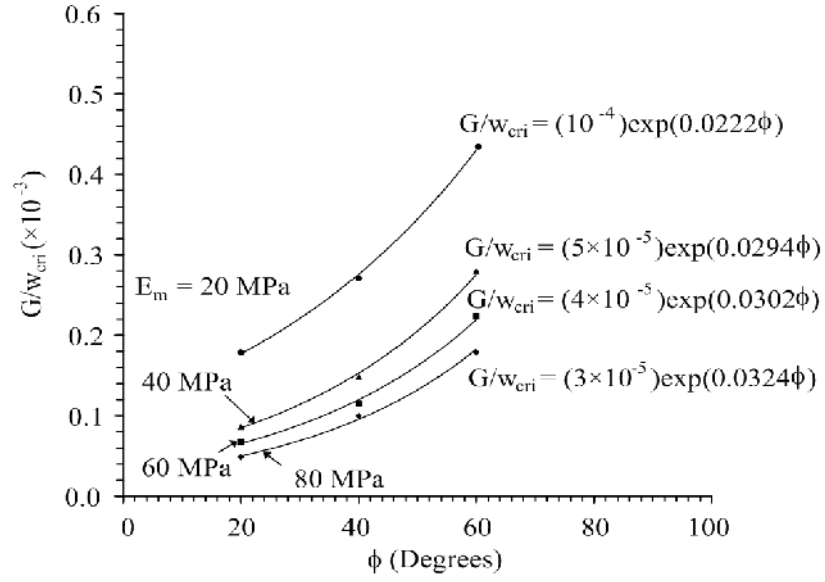
Figure 4.3 plots the maximum surface slope (G) normalized by the critical diameter (w_{cri}) as a function of the overburden friction angles (ϕ) for various deformation moduli (E_m). For each deformation modulus the normalized maximum slope (G/w_{cri}) increases with the friction angle, which can be represented by an exponential equation. Their empirical constants A_0 and B_0 depend on the deformation modulus. A power equation can be used to correlate A_0 and B_0 with the deformation modulus E_m , as shown in Figure 4.3. The normalized maximum slope can be expressed as:

$$G / w_{cri} = 0.0012 E_m^{-0.849} \exp(0.0103 \phi E_m^{0.27}) \quad (4.5)$$

The cavern depth at the critical condition decreases with increasing deformation modulus (Figure 4.4). The depth normalized by the critical diameter (d/w_{cri}), can be expressed as a function of E_m as:

$$d / w_{cri} = (-0.0213 \phi^{-0.636}) E_m + 1.55 \exp(-0.0163 \phi) \quad (4.6)$$

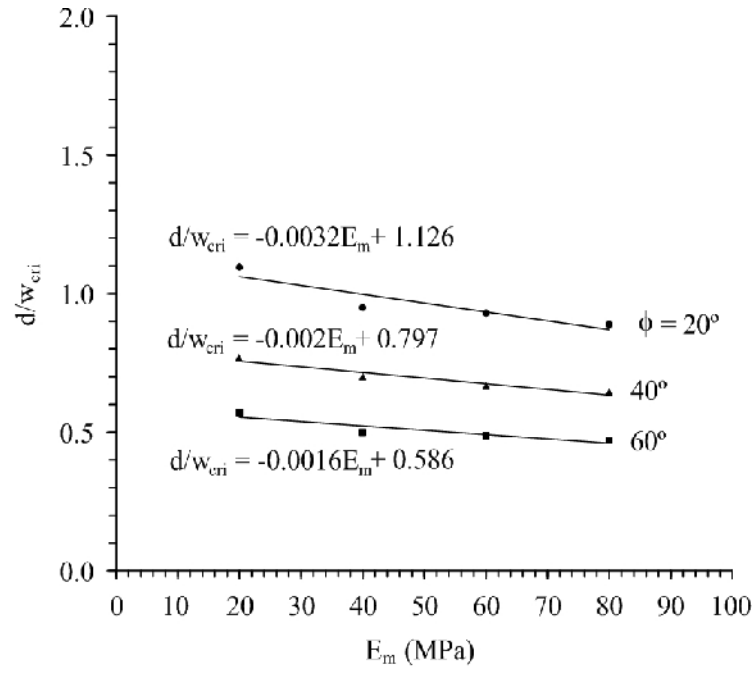
Similar to the derivation above, the relationships for the vertical deformation of the cavern roof (R_s) and the radius of influence on the surface ($B/2$) can also be developed (Figures 4.5 and 4.6).



$$G/w_{cri} = A_0 \cdot \exp(B_0 \phi), \text{ where; } A_0 = \alpha_{A0} \cdot E_m^{\beta_{A0}}; B_0 = \alpha_{B0} \cdot E_m^{\beta_{B0}}$$

| E_m (MPa) | A_0 | α_{A0} | β_{A0} | B_0 | α_{B0} | β_{B0} |
|-------------|--------------------|---------------|--------------|--------|---------------|--------------|
| 20 | 10^{-4} | 0.0012 | -0.849 | 0.0222 | 0.0103 | 0.27 |
| 40 | 5×10^{-5} | | | 0.0294 | | |
| 60 | 4×10^{-5} | | | 0.0302 | | |
| 80 | 3×10^{-5} | | | 0.0324 | | |

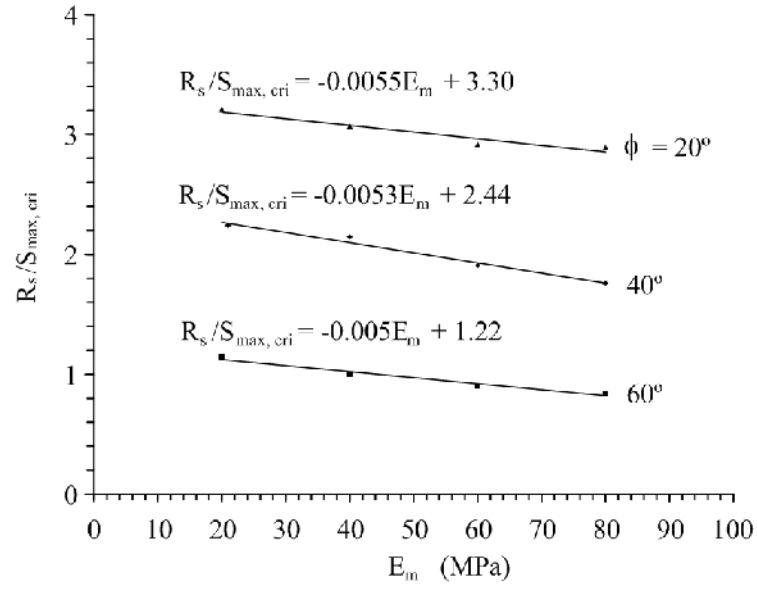
Figure 4.3 Maximum slope to critical cavern width ratio (G/w_{cri}) as a function of friction angle (ϕ) for various deformation moduli (E_m). A_0 , B_0 , α_{A0} , β_{A0} , α_{B0} and β_{B0} are empirical constants.



$$d/w_{cri} = -A_1 \cdot E_m + B_1, \text{ where; } A_1 = \alpha_{A1} \cdot \phi^{\beta_{A1}}; B_1 = \alpha_{B1} \cdot \exp(\beta_{B1} \cdot \phi)$$

| ϕ (Degrees) | A_1 | α_{A1} | β_{A1} | B_1 | α_{B1} | β_{B1} |
|------------------|--------|---------------|--------------|-------|---------------|--------------|
| 20 | 0.0032 | 0.0213 | -0.636 | 1.126 | 1.55 | -0.0163 |
| 40 | 0.0020 | | | 0.797 | | |
| 60 | 0.0016 | | | 0.586 | | |

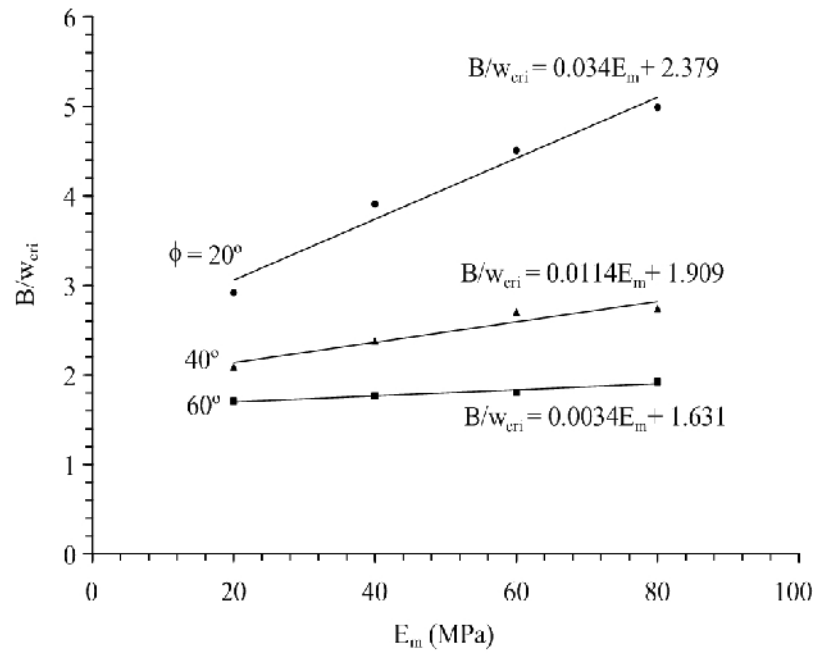
Figure 4.4 Cavern depth to critical cavern width ratio (d/w_{cri}) as a function of deformation modulus (E_m) for various friction angles (ϕ). A_1 , B_1 , α_{A1} , β_{A1} , α_{B1} and β_{B1} are empirical constants.



$$R_s/S_{\max, \text{cri}} = -A_2 \cdot E_m + B_2, \text{ where; } A_2 = \alpha_{A2} \cdot \phi + \beta_{A2}; B_2 = \alpha_{B2} \cdot \phi + \beta_{B2}$$

| ϕ (Degrees) | A_2 | α_{A2} | β_{A2} | B_2 | α_{B2} | β_{B2} |
|------------------|--------|---------------|--------------|-------|---------------|--------------|
| 20 | 0.0055 | -10^{-5} | 0.0058 | 3.30 | -0.0519 | 4.393 |
| 40 | 0.0053 | | | 2.44 | | |
| 60 | 0.0050 | | | 1.22 | | |

Figure 4.5 Roof deformation to maximum subsidence ratio at critical condition ($R_s/S_{\max, \text{cri}}$) as a function of deformation modulus (E_m) for various friction angles. A_2 , B_2 , α_{A2} , β_{A2} , α_{B2} and β_{B2} are empirical constants.



$$B/w_{cri} = A_3 \cdot E_m + B_3, \text{ where; } A_3 = \alpha_{A3} \cdot \exp(\beta_{A3} \cdot \phi); B_3 = \alpha_{B3} \cdot \exp(\beta_{B3} \cdot \phi)$$

| ϕ (Degrees) | A_3 | α_{A3} | β_{A3} | B_3 | α_{B3} | β_{B3} |
|------------------|--------|---------------|--------------|-------|---------------|--------------|
| 20 | 0.0340 | 0.11 | -0.058 | 2.379 | 2.844 | -0.0094 |
| 40 | 0.0114 | | | 1.909 | | |
| 60 | 0.0034 | | | 1.631 | | |

Figure 4.6 Diameter of influence to critical cavern width ratio (B/w_{cri}) as a function of deformation modulus (E_m) for various friction angles. A_3 , B_3 , α_{A3} , β_{A3} , α_{B3} and β_{B3} are empirical constants.

$$R_s / S_{\max, \text{cri}} = (10^{-5} \phi - 0.0058) E_m - 0.0519 \phi + 4.393 \quad (4.7)$$

$$B / w_{\text{cri}} = 0.11 \exp(-0.058 \phi) E_m + 2.844 \exp(-0.0094 \phi) \quad (4.8)$$

The same procedure is used for the sub-critical condition. The correlation results are shown in Figures 4.7 through 4.9, and can be expressed by the following equations:

$$G / w = 0.0012 E_m^{-0.412} \cdot (S_{\max}^{0.36 E_m})^{0.12} \quad (4.9)$$

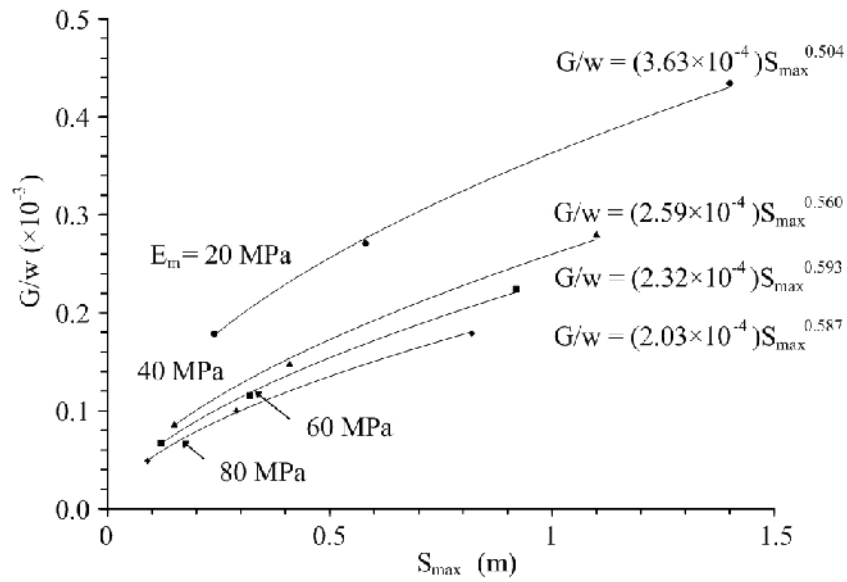
$$d / w = (-0.0002 E_m + 0.132) G^{(-0.7 E_m^{-0.1743})} \quad (4.10)$$

$$R_s / w = (0.205 E_m^{-0.701}) \cdot S_{\max}^{(0.0432 E_m^{0.386})} \quad (4.11)$$

The equations (4.5) through (4.11) are mainly result of this research that the relations can be connected between surface subsidence of the field data and cavern depth, cavern diameter and roof deformation are calculated with this equations.

4.4 Example of calculation

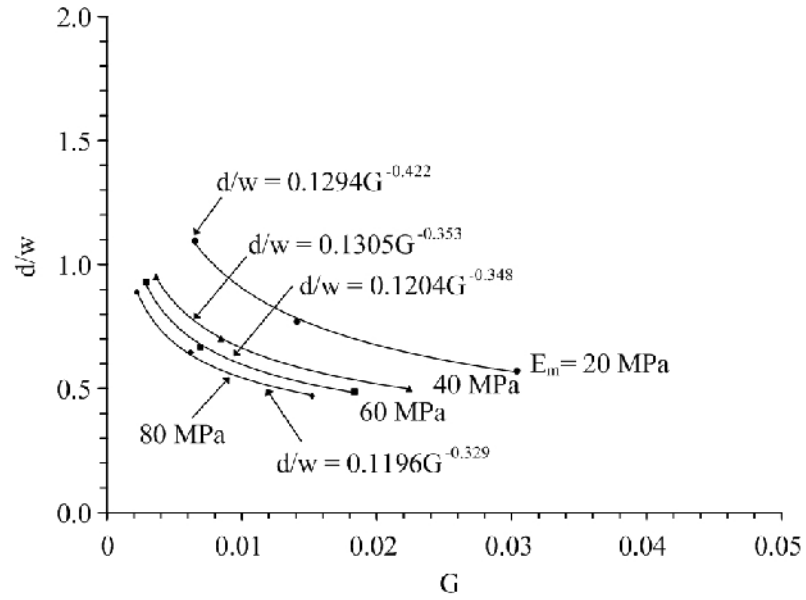
This section shows how to determine the cavern depth and diameter from an example set of survey data, as given in Table 4.1. The variables x_i , y_i are the local coordinates of point i , and z_i (equivalent to $S(r_i)$ in equation 4.1) is the vertical displacement at point i . Regression of these data using equation (4.1) results in a maximum subsidence at the center of the cavern equal to 0.46 m. Equation (4.3)



$$G/w = A_4 \cdot S_{\max}^{B_4}, \text{ where; } A_4 = \alpha_{A4} \cdot E_m^{\beta_{A4}}, B_4 = \alpha_{B4} \cdot E_m^{\beta_{B4}}$$

| E_m (MPa) | A_4 | α_{A4} | β_{A4} | B_4 | α_{B4} | β_{B4} |
|-------------|-----------------------|---------------|--------------|-------|---------------|--------------|
| 20 | 3.63×10^{-4} | 0.0012 | -0.412 | 0.504 | 0.36 | 0.12 |
| 40 | 2.59×10^{-4} | | | 0.560 | | |
| 60 | 2.32×10^{-4} | | | 0.593 | | |
| 80 | 2.03×10^{-4} | | | 0.587 | | |

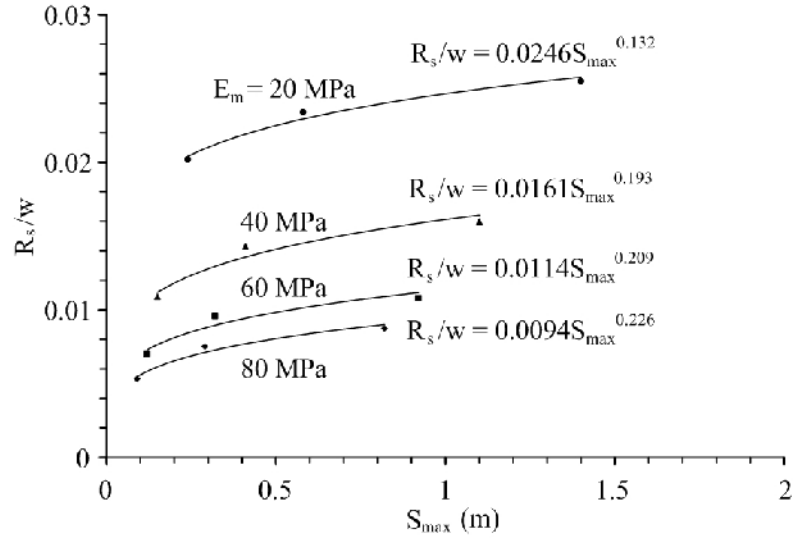
Figure 4.7 Maximum slope to cavern width ratio (G/w) as a function of maximum subsidence (S_{\max}) for various deformation moduli (E_m). A_4 , B_4 , α_{A4} , β_{A4} , α_{B4} and β_{B4} are empirical constants.



$$d/w = A_5 \cdot G^{-B_5}, \text{ where; } A_5 = \alpha_{A5} \cdot E_m + \beta_{A5}; B_5 = \alpha_{B5} \cdot E_m^{\beta_{B5}}$$

| E_m (MPa) | A_5 | α_{A5} | β_{A5} | B_5 | α_{B5} | β_{B5} |
|-------------|--------|---------------|--------------|-------|---------------|--------------|
| 20 | 0.1294 | -0.0002 | 0.132 | 0.422 | 0.7 | -1.743 |
| 40 | 0.1305 | | | 0.353 | | |
| 60 | 0.1204 | | | 0.348 | | |
| 80 | 0.1196 | | | 0.329 | | |

Figure 4.8 Cavern depth to cavern width ratio (d/w) as a function of maximum slope (G) for various deformation moduli (E_m). A_5 , B_5 , α_{A5} , β_{A5} , α_{B5} and β_{B5} are empirical constants.



$$R_s/w = A_6 \cdot S_{\max}^{B_6}, \text{ where; } A_6 = \alpha_{A6} \cdot E_m^{\beta_{A6}}, B_6 = \alpha_{B6} \cdot E_m^{\beta_{B6}}$$

| E_m (MPa) | A_6 | α_{A6} | β_{A6} | B_6 | α_{B6} | β_{B6} |
|-------------|--------|---------------|--------------|-------|---------------|--------------|
| 20 | 0.0246 | 0.205 | -0.701 | 0.132 | 0.0432 | 0.386 |
| 40 | 0.0161 | | | 0.193 | | |
| 60 | 0.0114 | | | 0.209 | | |
| 80 | 0.0094 | | | 0.226 | | |

Figure 4.9 Ratio of roof deformation to cavern width ratio (R_s/w) as a function of maximum subsidence (S_{\max}) for various deformation moduli (E_m). A_6 , B_6 , α_{A6} , β_{A6} , α_{B6} and β_{B6} are empirical constants.

Table 4.1 Example of ground survey data measured in subsiding area.

| i | x_i (m) | y_i (m) | z_i (m) |
|----|-----------|-----------|-----------|
| 1 | 2.5 | 0.0 | -0.400 |
| 2 | -2.5 | 2.5 | -0.400 |
| 3 | 5.0 | 0.0 | -0.400 |
| 4 | 3.0 | 4.0 | -0.450 |
| 5 | -5.0 | 5.0 | -0.450 |
| 6 | 10.0 | 0.0 | -0.450 |
| 7 | 6.0 | 8.0 | -0.470 |
| 8 | -10.0 | 0.0 | -0.470 |
| 9 | -6.0 | 8.0 | -0.390 |
| 10 | 0.0 | 10.0 | -0.390 |
| 11 | 9.0 | 12.0 | -0.390 |
| 12 | 0.0 | 15.0 | -0.390 |
| 13 | -12.0 | 9.0 | -0.390 |
| 14 | 20.0 | 0.0 | -0.420 |
| 15 | 12.0 | 16.0 | -0.420 |
| 16 | -12.0 | 16.0 | -0.270 |
| 17 | 0.0 | 20.0 | -0.270 |
| 18 | 25.0 | 0.0 | -0.270 |
| 19 | 15.0 | 20.0 | -0.270 |
| 20 | -25.0 | 0.0 | -0.270 |
| 21 | 0.0 | 30.0 | -0.270 |
| 22 | 35.0 | 0.0 | -0.250 |
| 23 | 0.0 | 35.0 | -0.250 |
| 24 | 40.0 | 0.0 | -0.250 |
| 25 | 45.0 | 0.0 | -0.150 |
| 26 | 0.0 | 45.0 | -0.150 |
| 27 | -30.0 | 40.0 | -0.150 |
| 28 | -54.7 | 0.0 | -0.050 |
| 29 | 0.0 | 54.7 | -0.050 |
| 30 | 48.0 | 64.0 | -0.015 |
| 31 | 0.0 | 80.0 | -0.015 |
| 32 | -48.0 | 64.0 | -0.015 |

determines the maximum slope at the inflection point as 0.013. This example assumes that the deformation modulus of the overburden is known and equal to 20 MPa, with a friction angle equal to 40° . This example assumes that the groundwater table is at the ground surface.

Under critical condition, the cavern diameter and depth can be estimated from equations (4.5) through (4.7), as 54.6 m and 41.9 m. The roof deformation and radius of influence are 1.02 m and 59.2 m. If the ground is under sub-critical condition, the cavern diameter and depth are predicted as 55.6 m and 43.2 m, with the roof deformation and radius of influence equal to 1.25 m and 60.3 m. It can be seen that the solutions are not unique depending on whether the cavern is under sub-critical or critical condition. The cavern diameter, roof deformation and radius of influence can however be calculated if the cavern depth can be pre-defined. Within the brine pumping areas the depth of the cavern roof or of the overburden-salt interface can often be determined from interpolating or extrapolating from the existing drill holes or brine pumping wells.

4.5 Super-critical condition

Two scenarios can occur when the subsidence reaches its super-critical condition (collapse of cavern roof and overburden), which is dictated by the cavern height. If the cavern height is equal to or less than the roof deformation, the immediate roof rock will touch the cavern floor. Vertical movement of the ground may or may not continue depending on whether the salt floor dissolution is continued. In this case the subsidence is likely to be small, the subsiding area is relatively flat, and development of a sinkhole is unlikely.

If the cavern height is however significantly greater than the critical roof deformation, failure of the cavern roof can occur under the super-critical condition. The failure can progress upward and may lead to a sinkhole development. In this case the cavern location can be evidently defined, but accurate prediction of the cavern diameter and depth is virtually impossible. Subsurface investigations by Jenkunawat (2005) and Wannakao and Walsri (2007) reveals that collapsing of the roof rock above some caverns in a brine pumping area has also resulted in a large void remaining in the overburden.

4.6 Discrete element analyses

The difficulty in predicting the cavern configurations under super-critical condition is due to the complexity of the post failure behavior of the rock mass and movement of the joint system. To demonstrate these issues discrete element analyses are performed using UDEC code (Itasca, 2004) to simulate the movement of the jointed rock mass above an isolated salt cavern. The discrete element models are constructed to represent a cavern dissolved at the overburden-salt interface. The cavern depth, diameter and height are maintained constant at 40 m, 100 m and 30 m, representing a super-critical condition. A hydrostatic stress is applied on both sides of the model. For the first series of simulations there are two mutually perpendicular joint sets inclined at 45° , with friction angles varying from 20° , 30° and 40° . The second series assesses the effect of joint orientation by using a constant joint friction angle of 30° , and varying the joint dips from 15° , 30° to 45° . The joint spacing for both cases is 8 m.

Simulation results from the first series (shown in Figure 4.10), suggest that even under the same cavern geometry and joint orientation, different joint friction angles can cause significantly different post-failure conditions. For the overburden with low-

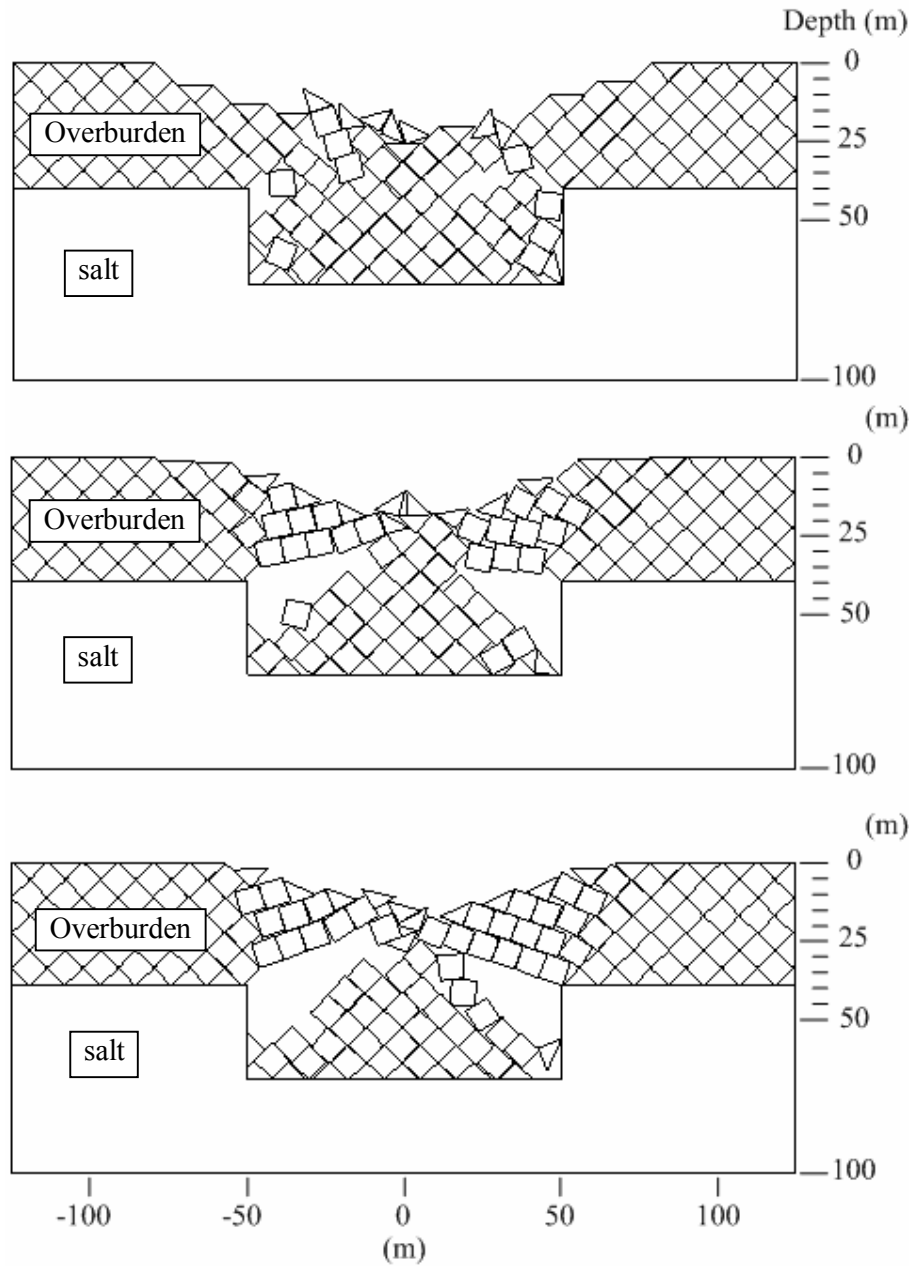


Figure 4.10 UDEC simulations for cavern roof failure for joints with friction angles of 20° (top), 30° (middle) and 40° (bottom). $H = 30$ m, $d = 40$ m, $w = 100$ m.

friction joints, the cavern can be completely filled with the collapsing rock blocks. This results in a deep sinkhole or a large depression area, or both. Gaps or voids can be formed if the overburden has joints with a higher friction angle, resulting in a shallower sinkhole and smaller subsiding area.

For the second series, Figure 4.11 compares the simulated results under the same joint friction ($\phi = 30^\circ$) but different joint angles. Different patterns of block collapsing can be obtained for the joints with 30° and 45° inclinations. It is interesting to observe that with the joint angle of 15° the roof failure does not progress upward, and has virtually no impact on the ground surface.

To cover and understand the effects of cavern height and cavern diameter, the third and fourth series of the simulation are made. For the third series (as shown in Figure 4.12) of simulations there are two mutually perpendicular joint sets inclined at 45° , with cavern diameter varying from 50, 75 to 100 m. The cavern height and depth are maintained constant at 30 m and 40 m. For the fourth series (as shown in Figure 4.13) the cavern height varies from 10, 20 to 30 m with the cavern depth of 40 m and joint orientations of 45° . The results of both series indicate that, if the cavern diameter increases, the larger the cavern, the higher possibility of developing a sinkhole. On the other hand, if cavern height increases, a larger maximum subsidence will be obtained.

The numerical simulations under the assumed joint conditions above clearly demonstrate the complexity and uncertainty of the subsidence under super-critical condition which can not be easily determined by the analytical method proposed here. Detailed subsurface investigation is required to understand the failure and movement of the overburden under the super-critical condition.

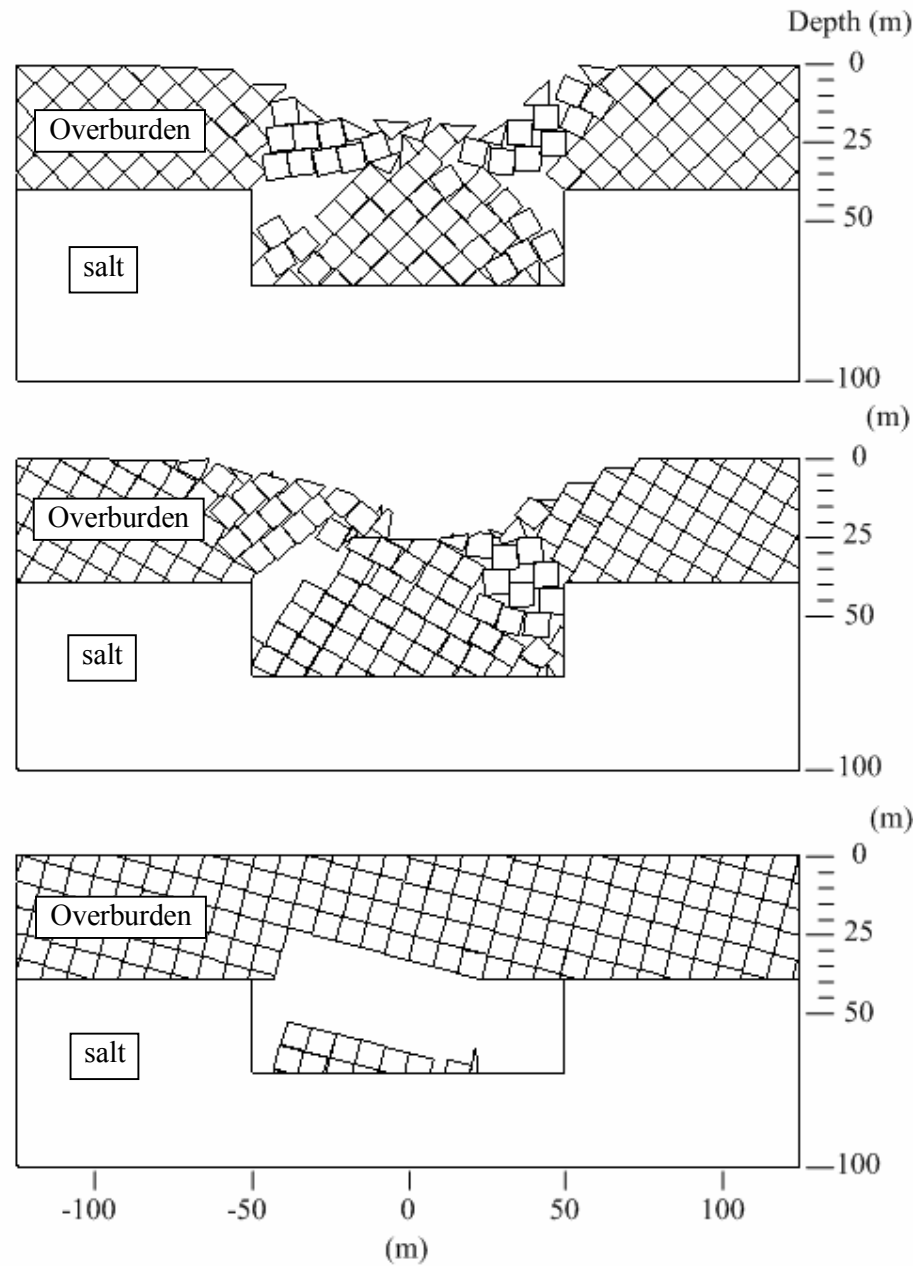


Figure 4.11 UDEC simulations for cavern roof failure with joint dip angles of 45° (top), 30° (middle) and 15° (bottom). $H = 30$ m, $d = 40$ m, $w = 100$ m.

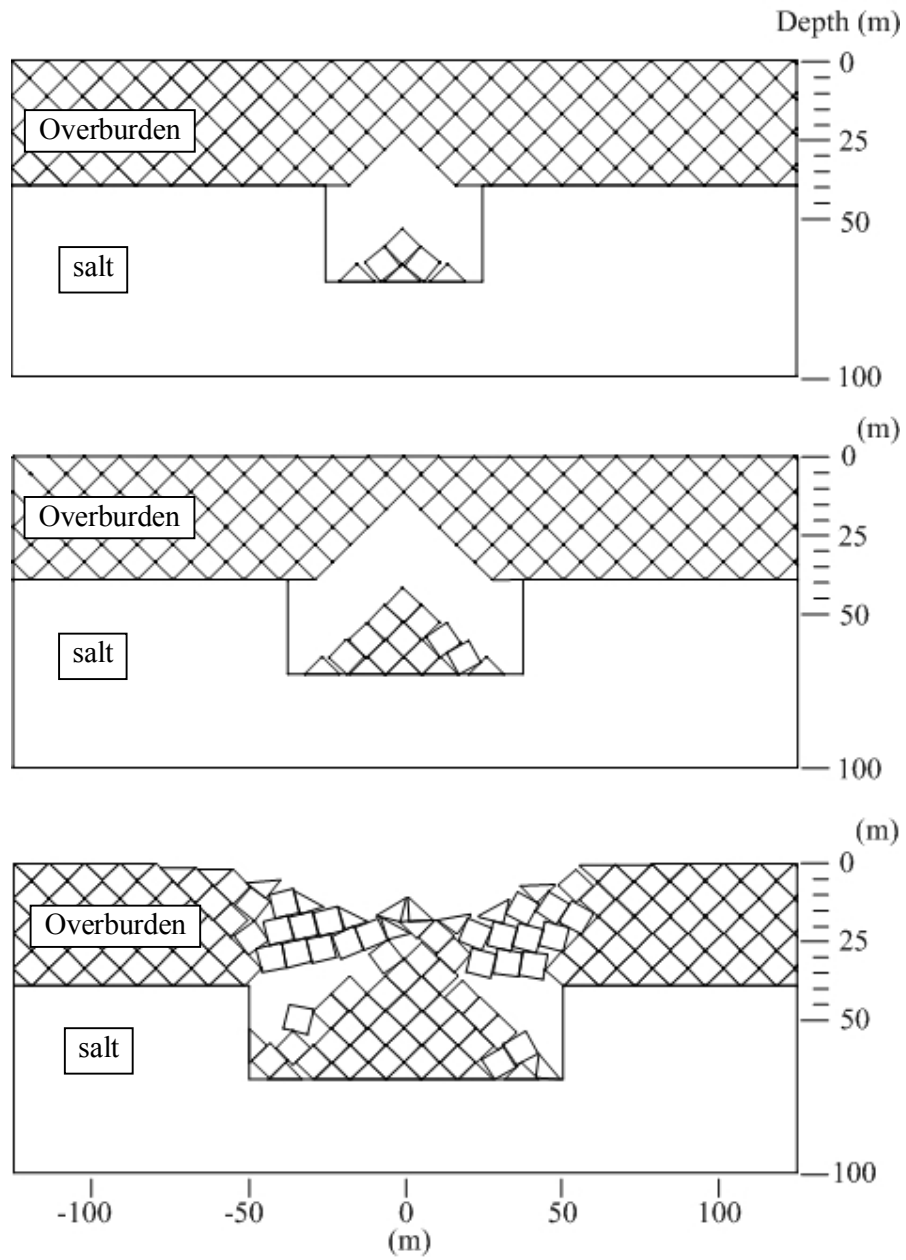


Figure 4.12 UDEC simulations for cavern roof failure with cavern diameter of 50 m (top), 75 m (middle) and 100 m (bottom). $H = 30$ m, $d = 40$ m, joint dip = 45° .

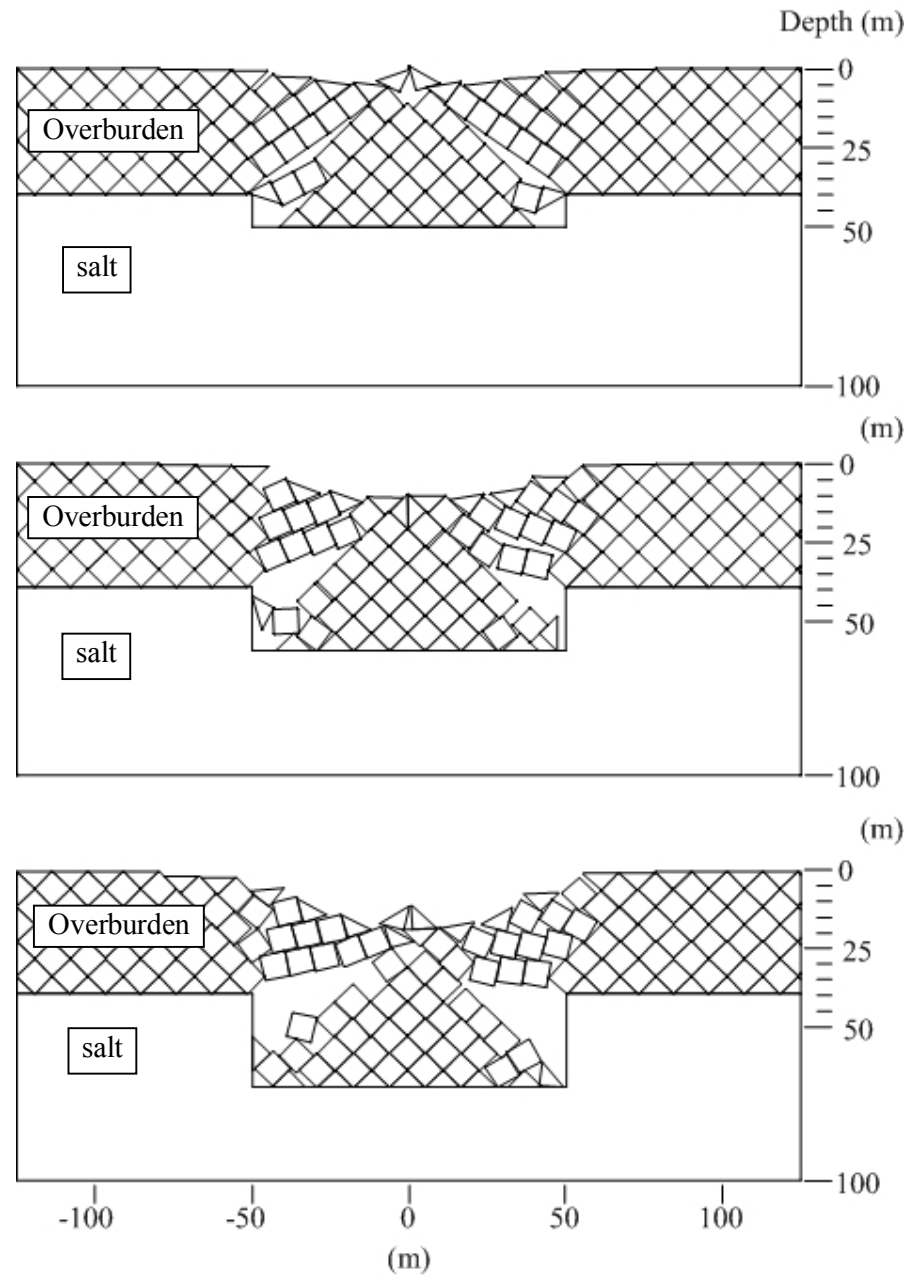


Figure 4.13 UDEC simulations for cavern roof failure with cavern height of 10 m (top), 20 m (middle) and 30 m (bottom). $d = 40$ m, $w = 100$ m, joint dip = 45° .

4.7 Field investigations

Field investigations are made at Nonsabang village, Nongkwang village, Bodaeng village, Banmuang district, Sakon Nakhon province, Bandung Tambol, Banchai Tambol, Bandung district, Udon Thani province, and Phon Phisai district, Nongkhai province (2 – 3 April 2009) to verify the program. The results from the investigations do not give useful information to verify the program. This is because the subsidence areas and sinkholes were flooded and backfilled with top soil (by human). The local peoples in brine pumping industry not permit to enter and conduct any field survey in the area. Figures 4.14 through 4.16 show some sinkholes at Nonsabang village, Banmuang district, Sakon Nakhon province, found during the field investigation.



Figure 4.14 Some sinkhole cause by brine pumping at Nonsabang village, Banmuang district, Sakon Nakhon province.



Figure 4.15 Some sinkhole caused by brine pumping at Nonsabang village, Banmuang district, Sakon Nakhon province.



Figure 4.16 Very big sinkhole caused by brine pumping at Nonsabang village, Banmuang district, Sakon Nakhon province.

CHAPTER V

CONCLUSIONS AND RECOMMENDATIONS FOR FUTURE STUDIES

5.1 Conclusions

Regression analysis of the ground survey data can provide a smooth and representative profile of the surface subsidence which agrees reasonably well with the hyperbolic function proposed by Singh (1992). An analytical method developed from the results of finite difference analyses can be used to determine the cavern depth and diameter under sub-critical and critical conditions. The two conditions can be distinguished if the cavern depth is known, in most cases probably by interpolating between nearby boreholes or exploratory wells.

Accuracy of the prediction depends on the number of the field measurements used in the regression analyses, the uniformity of the properties of the overburden areas, and the configurations of the caverns.

The correlations of the subsidence components with the overburden mechanical properties and cavern geometry are applicable to the range of site conditions specifically imposed here (e.g., half oval-shaped cavern created at the overburden-salt interface, horizontal rock units, flat ground surface, and saturated condition). These relations may not be applicable to subsidence induced under different rock characteristics or different configurations of the caverns.

The proposed method is not applicable under super-critical conditions where post-failure behavior of the overburden rock mass is not only unpredictable but also complicated by the system of joints, as demonstrated by the results of the discrete element analyses.

The proposed method is useful as a predictive tool to identify the configurations of a solution cavern and the corresponding subsidence components induced by the brine pumping practices. Subsequently, remedial measure can be implemented to minimize the impact from the cavern development before severe subsidence or sinkhole occurs.

5.2 Recommendations for future studies

The scope of this research is relatively narrow, emphasizing on the correlations between the surface profile and the cavern configurations. This leads to the following research needs.

Computer program developed here for prediction of cavern configurations should be examined and verified with the field measurements to adjust the parameters (e.g. the properties of the overburden based on laboratory testing). After a field verification is made, the mathematical forms can be altered, if deem necessary to ensure that the relations between surface characteristics and the cavern configurations are appropriate and adequate.

Subsurface examination should be conducted to reveal the common shape of the solution cavern at the salt – overburden interface. The effect of topography and inclination of contact surface should also be studied.

Subsurface investigation (Geophysical survey e.g. resistivity, seismic) is required to understand the behavior of failure and movement of the overburden under the super-critical condition.

REFERENCES

- Asadi, A., Shahriar, K., Goshtasbi, K., and Najm, K. (2005). Development of new mathematical model for prediction of surface subsidence due to inclined coal-seam mining. **J. S. Afr. Inst. Min. Metall.** Vol. 105(11) : 15-20.
- Barton, N.R. (1974). **A review of the shear strength of filled discontinuities in rock.** Norwegian Geotech. Inst. Publ. No. 105. Oslo: Norwegian Geotech. Inst.
- Crosby, K. (2007). Integration of rock mechanics and geology when designing the Udon South sylvinitic mine. **Proceedings of the First Thailand Symposium on Rock Mechanics**, Nakhon Ratchasima: Suranaree University of Technology. pp. 3-22.
- Cui, X., Miao, X., Wang, J., Yang, S., Liu, H., Song, Y., Liu, H., and Hu, X. (2000). Improved prediction of differential subsidence caused by underground mining. **Int. J. Rock Mech. Min. Sci.**, Vol. 37(4) : 615-627.
- Fuenkajorn, K. (2002). Design guideline for salt solution mining in Thailand, **Research and Development Journal of the Engineering Institute of Thailand**, Vol. 13(1) : 1-8.
- Grøneng, G., Nilsen, B., and Sandven, R. (2009). Shear strength estimation for Åknes sliding area in western Norway. **Int. J. Rock Mech. Min. Sci.**, Vol. 46(3) : 479-488.
- Itasca (1992a). **FLAC—Fast Lagrangian Analysis of Continua, Version 4.0**, User Manual. Itasca Consulting Group Inc., Minneapolis, MN, USA.

- Itasca (1992b). **User manual for FLAC–Fast Langrangian Analysis of Continua, Version 4.0**, Itasca Consulting Group Inc., Minneapolis, MN.
- Japakasetr, T. (1985). Review on rock salt and potash exploration in Northeast Thailand, **Conference on Geology and Mineral Resources Development of the Northeast, Thailand, 26-29 November 1985**, Thailand: Khon Kaen University, pp. 135-147.
- Japakasetr, T. (1992). Thailand's mineral potential and investment opportunity, **National Conference on Geologic Resources of Thailand: Potential for Future Development**, November 1992, DMR, Bangkok, Thailand, pp. 641-652.
- Japakasetr, T. and Suwanich, P. (1982). Potash and Rock Salt in Thailand Appendix A Nonmetallic Minerals Bulletin No. 2, **Economic Geology Division, Department of Mineral Resources, Bangkok, Thailand**, pp. A1-A252.
- Japakasetr, T. and Workman, D. R. (1981). Evaporite deposits of northeast Thailand, **Circum-Pacific Conferences**, Hawaii, pp. 179-187.
- Jenkunawat, P. (2005). Results of drilling to study occurrence of salt cavities and surface subsidence Ban Non Sabaeng and Ban Nong Kwang, Amphoe Ban Muang, Sakon Nakhon. **International Conference on Geology, Geotechnical and Mineral Resources of Indochina (GEOINDO 2005)**, Khon Kaen: Khon Kaen University. pp. 259-267.
- Jenkunawat, P. (2007). Results of drilling to study occurrence of salt cavities and surface subsidence Ban Non Sabaeng and Ban Nong Kwang, Sakon Nakhon. **Proceedings of the First Thailand Symposium on Rock Mechanics**, Nakhon Ratchasima: Suranaree University of Technology. pp. 257-274.

- Nieland, J. D. (1991). **SALT_SUBSID: A PC-Based Subsidence Model**. Solution Mining Research Institute, Report No. 1991-2-SMRI, California, USA, 67pp.
- Rattanajarurak, P. (1990). **Formation of The Potash Deposits, Khorat Plateau, Thailand**. M.S. Thesis, School of Mine, Kensington, Australia.
- Sattayarak, N. (1983). Continental Mesozoic stratigraphy of Thailand, **Symposium on Stratigraphy of Thailand**, 18-19 November, Bangkok, pp. 77-80.
- Sattayarak, N. (1983). Review of continental Mesozoic stratigraphy of Thailand: **Proceeding Stratigraphic correlation of Thailand and Malaysia**, Geol. Soc. Thailand, Vol. 1 : 127-148.
- Sattayarak, N. (1985). Review on Geology of Khorat plateau, **Conference on Geology and Mineral Resources Development of the Northeast, Thailand 26-29 November 1985**, Thailand: Khon Kaen University, pp. 23-30.
- Sattayarak, N. and Polachan, S. (1990). Rock salt beneath the Khorat plateau (in Thai), In **Proceedings of the Conference on Geology and Mineral Resources of Thailand** (pp. 1-14). Bangkok, Thailand: Department of Mineral Resources.
- Sattayarak, N., Chaisilboon, B., Srikulwong, S., Charusirisawat, R., Mahattanachai, T. and Chantong, W. (1998). Tectonic evolution and basin development of the northeast Thailand, **Seminar on Mesozoic Redbeds in the Northeastern Thailand**, August 28, pp. 1-19.
- Shu, D.M., and Bhattacharyya, A.K. (1993). Prediction of sub-surface subsidence movements due to underground coal mining. **Geotechnical and Geological Engineering**. Springer Netherlands. Vol. 11(4) : 221-234.

- Singh, M. M. (1992). Mine Subsidence. **SME Mining Engineering Handbook**. Hartman, H. L. (ed). (pp.938-971). Society for mining metallurgy and exploration, Inc Colorado.
- Supajanya, T., Vichapan, K. and Sri-israporn, S. (1992). Surface expression of shallow salt dome in Northeast Thailand, **National Conference on Geologic Resources of Thailand**: Potential for Future Development, 17-24 November 1992, DMR, Bangkok, Thailand, pp. 89-95.
- Suwanich, P. (1978). **Potash in northeastern of Thailand (in Thai)**. **Economic Geology Document No. 22**. Bangkok: Economic Geology, Division, Department of Mineral Resources.
- Suwanich, P. (1982). **Potash and rock salt in Thailand**. **Nonmetallic Mineral Bulletin No.2**, Bangkok: Economic Geology Division, Department of Mineral Resources, Bangkok, Thailand.
- Suwanich, P. (1986). **Potash and Rock Salt in Thailand : Nonmetallic Minerals Bulletin No.2**, Economic Geology Division, Department of Mineral Resources, Bangkok, Thailand.
- Thiel, K and Zabuski, L. (1993). Rock mass investigations in hydroengineering. **Comprehensive Rock Engineering**. Hudson, J.A. (ed). London: Pergamon Press, Vol. 3 : 839-861.
- Utha-aroon, C. (1993). Continental origin of the Maha Sarakham evaporites, Northeastern Thailand, **Journal of Southeast Asian Earth Sciences**, 1993, Great Britain, Vol. 8(1-4) : 193-203.

- Vattanasak, H. (2006). **Salt reserve estimation for solution mining in the Khorat basin**, M.Eng. Thesis, Nakhon Ratchasima: Suranaree University of Technology.
- Wannakao, L. and Walsri, C. (2007). Subsidence models in salt production area. **Proceedings of the First Thailand Symposium on Rock Mechanics**, Nakhon Ratchasima: Suranaree University of Technology. pp. 311-321.
- Wannakao, L., Janyakorn, S., Munjai, D., and Vorarat, A. (2004). **Geological and geotechnical properties analysis of overburden and salt formations in the northeast for surface subsidence model**, final research report, Department of Geotechnology, Khon Kaen University, 70pp. (in Thai)
- Wannakao, L., Munjai, D., and Janyakorn, S. (2005). Geotechnical investigation of surface subsidence at Ban Non Sabaeng salt production area, Sakon Nakhon, Thailand. **International Conference on Geology, Geotechnical and Mineral Resources of Indochina (GEOINDO 2005)**. Khon Kaen: Khon Kaen University. p. 282.
- Warren, J. (1999). **Evaporites: Their Evolution and Economics**, Blackwell Science, 438pp.
- Yumuang, S. (1983). **On the origin of evaporite deposits in the maha sarakham formation in Bamnet Narong area, Changwat Chaiyaphum**, M.S. thesis, Chulalongkorn University, Thailand.
- Yumuang, S., Khantapab, C., and Taiyagupt, M. (1986). The evaporate deposits in Bamnet Narong area, Northeastern Thailand, In **Proceedings of the GEOSEA V** (Bulletin 20, Vol. 2, pp. 249-267). Geological Society of Malaysia.

APPENDIX A

SOURCE CODE

```

#ifndef HYPERBOLIC_TANGENT_SURFACE_FITTING
#define HYPERBOLIC_TANGENT_SURFACE_FITTING

#include "scattered_data.h"
#include <windows.h>

class ctanh
{
public:
    ctanh ();
    ~ctanh ();
public:
    void      init (Cscattereddata *pdata);
    void      fittanh (void);
    int       isready (void) { return m_isready; }
    void      interp (double mu [2], double mf [3], double mn [3]);
    void      interp (double r, double *s, double *n, double *c);
    void      drawRGBplot (HDC hdc, int scale);
    void      exportcoefficient (const char *lpszpath);

public:
    void      gettanh (double a [6]);

public:
    double     E (double p []);
    double     dE (double p []);

    double     dE0 (double p []);
    double     dE1 (double p []);
    double     dE2 (double p []);
    double     dE3 (double p []);
    double     dE4 (double p []);
    double     dE5 (double p []);

protected:
    double     estimatedtanh (double p [], double r);
    void       locatedatacentroid (void);

public:
    Cscattereddata *m_pdata;

protected:
    double     m_ct [6]; // hyperbolic tangent coefficients
    double     m_cg [2]; // data centroid
    int        m_isready;
};
#endif

```

```

#include <stdio.h>
#include <float.h>
#include <math.h>
#include "tanh.h"
#include "goptimal.h"

static ctanh      *localtanh      = NULL;
double            localE (double p []);
double            localdE (int i, double p []);

// BEGIN of local objective functions
double localE (double p [])
{
    return localtanh->E (p);
}

double localdE (int i, double p [])
{
    double ret = 0.0;

    switch (i)
    {
        case 0 : ret = localtanh->dE0 (p);
                  break;

        case 1 : ret = localtanh->dE1 (p);
                  break;

        case 2 : ret = localtanh->dE2 (p);
                  break;

        case 3 : ret = localtanh->dE3 (p);
                  break;

        case 4 : ret = localtanh->dE4 (p);
                  break;

        case 5 : ret = localtanh->dE5 (p);
                  break;
    }

    return ret;
}

// END of local objective functions

ctanh::ctanh ()
{

```



```

        init (NULL);
    }

ctanh::~~ctanh ()
{
}

inline double ctanh::estimatedtanh (double p [], double r)
{
    return p [0]*tanh (p [1]*10.0*r - p [2]) + p [3];
}

double ctanh::E (double p [])
{
    double      ui [ 2], fi [3];
    double error, delta, rx, ry, r;
    long  i, ncount;

    ncount = m_pdata->getcount ();
    for (i = 0, error = 0.0; i < ncount; i++)
    {
        m_pdata->getdata (i, ui, fi);

        rx      = ui [0] - p [4];
        ry      = ui [1] - p [5];
        r       = sqrt (rx*rx + ry*ry);

        delta   = fi [2] - estimatedtanh (p, r);
        error   = error + delta*delta;
    }

    return error;
}

// derivative wrt. the amplitude
double ctanh::dE0 (double p [])
{
    double      ui [ 2], fi [3];
    double error, delta, r, rx, ry;
    long  i, ncount;

    ncount = m_pdata->getcount ();

    for (i = 0, error = 0.0; i < ncount; i++)
    {
        m_pdata->getdata (i, ui, fi);

```

```

        rx          = ui [0] - p [4];
        ry          = ui [1] - p [5];
        r           = sqrt (rx*rx + ry*ry);

        delta      = tanh (p [1]*10.0*r - p [2])*(fi [2] - estimatedtanh (p, r));
        error      = error - delta;
    }

    return error;
}

// derivative wrt. the radian coefficient
double ctanh::dE1 (double p [])
{
    double      ui [ 2], fi [3];
    double error, delta, r, rx, ry, sech2;
    long   i, ncount;

    ncount = m_pdata->getcount ();

    for (i = 0, error = 0.0; i < ncount; i++)
    {
        m_pdata->getdata (i, ui, fi);

        rx          = ui [0] - p [4];
        ry          = ui [1] - p [5];
        r           = sqrt (rx*rx + ry*ry);

        sech2      = 1.0 - pow (tanh (p [1]*10.0*r - p [2]), 2.0);
        delta      = (p [0]*10.0*r*sech2)*(fi [2] - estimatedtanh (p, r));
        error      = error - delta;
    }

    return error;
}

// derivative wrt. the radian offset
double ctanh::dE2 (double p [])
{
    double      ui [ 2], fi [3];
    double error, delta, r, rx, ry, sech2;
    long   i, ncount;

    ncount = m_pdata->getcount ();

    for (i = 0, error = 0.0; i < ncount; i++)
    {

```

```

m_pdata->getdata (i, ui, fi);

    rx          = ui [0] - p [4];
    ry          = ui [1] - p [5];
    r           = sqrt (rx*rx + ry*ry);

    sech2       = 1.0 - pow (tanh (p [1]*10.0*r - p [2]), 2.0);
    delta       = (p [0]*(-1.0)*sech2)*(fi [2] - estimatedtanh (p, r));
    error       = error - delta;
}

return error;
}

// derivative wrt. the function offset
double ctanh::dE3 (double p [])
{
    double      ui [ 2], fi [3];
    double error, delta, r, rx, ry;
    long  i, ncount;

    ncount = m_pdata->getcount ();

    for (i = 0, error = 0.0; i < ncount; i++)
    {
        m_pdata->getdata (i, ui, fi);

        rx          = ui [0] - p [4];
        ry          = ui [1] - p [5];
        r           = sqrt (rx*rx + ry*ry);

        delta       = (1.0)*(fi [2] - estimatedtanh (p, r));
        error       = error - delta;
    }

    return error;
}

// derivative wrt. the x-centriod
double ctanh::dE4 (double p [])
{
    double      ui [ 2], fi [3];
    double error, delta, r, rx, ry, sech2;
    long  i, ncount;

    ncount = m_pdata->getcount ();

```

```

        for (i = 0, error = 0.0; i < ncount; i++)
        {
            m_pdata->getdata (i, ui, fi);

            rx          = ui [0] - p [4];
            ry          = ui [1] - p [5];
            r           = sqrt (rx*rx + ry*ry);

            if (r > 0.0)
            {
                sech2 = 1.0 - pow (tanh (p [1]*10.0*r - p [2]), 2.0);
                delta  = (p [0]*10.0*p [1]*sech2*(-rx/r))*(fi [2] - estimatedtanh
(p, r));
                error  = error - delta;
            }
        }

        return error;
    }

// derivative wrt. the x-centriod
double ctanh::dE5 (double p [])
{
    double    ui [ 2], fi [3];
    double error, delta, r, rx, ry, sech2;
    long      i, ncount;

    ncount = m_pdata->getcount ();

    for (i = 0, error = 0.0; i < ncount; i++)
    {
        m_pdata->getdata (i, ui, fi);

        rx          = ui [0] - p [4];
        ry          = ui [1] - p [5];
        r           = sqrt (rx*rx + ry*ry);

        if (r > 0.0)
        {
            sech2 = 1.0 - pow (tanh (p [1]*10.0*r - p [2]), 2.0);
            delta  = (p [0]*10.0*p [1]*sech2*(-ry/r))*(fi [2] - estimatedtanh
(p, r));
            error  = error - delta;
        }
    }

    return error;
}

```

```

}

void ctanh::locatedatacentroid (void)
{
    long    i, ncount;
    double ui [2], fi [3];

    ncount = m_pdata->getcount ();
    for (i = 0, m_cg [0] = m_cg [1] = 0.0; i < ncount; i ++)
    {
        m_pdata->getdata (i, ui, fi);

        m_cg [0] += ui [0];
        m_cg [1] += ui [1];
    }

    m_cg [0] /= (double) ncount;
    m_cg [1] /= (double) ncount;
}

void ctanh::init (Cscattereddata *pdata)
{
    m_pdata = pdata;

    //      initialise the tanh constants to unity
    for (int i = 0; i < 6; i ++)
        m_ct [i] = 1.0;

    //      locate centroid (DC offset) of the data
    if (pdata)
        locatedatacentroid ();

    m_isready    = 0;
}

void ctanh::fittanh (void)
{
    long                i, ncount = m_pdata->getcount ();
    double              maxs, ct [6], scoef;
    CGradientOptimiser thegrad (localE, localdE, 6);

    //      initialise the tanh constants to unity
    for (i = 0; i < 4; i ++)
        ct [i] = 1.0;

    ct [4] = m_cg [0];
    ct [5] = m_cg [1];

```

```

    localtanh      = this;
    maxs           = 0.25;

    // run the steepest descent to get the estimate
    thegrad.setminmax (-10.0, 10.0);
    thegrad.init (ct);
    thegrad.setoptparams (maxs, 1.0E-4*maxs, 1.0E-6*maxs);
    thegrad.setmaxit (5000);
    thegrad.runconjugategradient ();
    // thegrad.runsteepestdescent ();
    thegrad.optimum (ct);

    // run the conjugate gradient to get the accurate results
    for (scoef = 1.0; scoef >= 0.125; scoef = 0.5*scoef)
    {
        thegrad.init (ct);
        thegrad.setoptparams (scoef * maxs, 1.0E-6*scoef*maxs, 1.0E-
8*scoef*maxs);
        thegrad.setmaxit (1000);
        thegrad.runconjugategradient ();
        thegrad.optimum (ct);
    }

    for (i = 0; i < 6; i++)
        m_ct [i] = ct [i];

    m_cg [0] = m_ct [4];
    m_cg [1] = m_ct [5];

    m_isready = 1;
/*
    FILE                *fp;
    double               rx, ry, r;
    double               ui [2], fi [3];

    fp = fopen ("c:\\test80.txt", "wt");

    fprintf (fp, "%8.4f\t%8.4f\t%8.4f\t%8.4f\t%8.4f\t%8.4f\n", ct [0], ct [1], ct [2],
ct [3], ct [4], ct [5]);
    for (i = 0; i < ncount; i++)
    {
        m_pdata->getdata (i, ui, fi);

        rx                = ui [0] - m_cg [0];
        ry                = ui [1] - m_cg [1];
        r                 = sqrt (rx*rx + ry*ry);

```

```

        fprintf (fp, "%8.4f\t%8.4f\t%8.4f\n", r, fi [2], estimatedtanh (ct, (float)
r));
    }
    fclose (fp);
*/
}

void ctanh::interp (double r, double *s, double *n, double *c)
{
    double arg, htan, sech2;

    if (m_isready)
    {
        arg      = m_ct [1]*10.0*r - m_ct [2];
        htan     = tanh (arg);
        sech2    = 1.0 - htan*htan;

        *s       = m_ct [0]*htan + m_ct [3];
        *n       = m_ct [0]*m_ct [1]*10.0*sech2;
        *c       = -m_ct [0]*m_ct [1]*m_ct [1]*100.0*htan/cosh (arg);
    }
}

void ctanh::gettanh (double a [6])
{
    for (int i = 0; i < 6; i++)
        a [i] = m_ct [i];
}

void ctanh::interp (double mu [2], double mf [3], double mn [3])
{
    double va [3], vb [3], rx, ry, r, sech2, delbr;

    if (m_isready)
    {
        mf [0]    = mu [0];
        mf [1]    = mu [1];

        rx       = mu [0] - m_cg [0];
        ry       = mu [1] - m_cg [1];
        r        = sqrt (rx*rx + ry*ry);

        mf [2]    = estimatedtanh (m_ct, (float) r);
        sech2     = 1.0 - pow (tanh (m_ct [1]*10.0*r - m_ct [2]), 2.0);
        delbr     = m_ct [0]*m_ct [1]*10.0*sech2;

        va [0] = 1.0;

```

```
va [1] = 0.0;
    va [2] = r > 0.0 ? delbr*rx/r : 0.0;

vb [0] = 0.0;
vb [1] = 1.0;
vb [2] = r > 0.0 ? delbr*ry/r : 0.0;

mn [0] = va [1] * vb [2] - va [2] * vb [1];
mn [1] = va [2] * vb [0] - va [0] * vb [2];
mn [2] = va [0] * vb [1] - va [1] * vb [0];
    }
}
```


APPENDIX B

USER MANUAL

USER MANUAL

This program is separated into two parts; (1) regression analysis (written in C language), and 2) solution cavern dimension calculation (written in Microsoft excel). This program can be used to calculate the subsidence components and the location, depth and size of caverns created at the interface between salt and overlying formations under sub-critical and critical conditions. The procedure is as follows:

- 1) Install the “Saltsurf” program and “Predict Cavern.xls” into your computer.
- 2) Open program “Saltsurf”.
- 3) Click “open” on the right window command and input the survey data (the data are in x, y and z coordinates in subsidence areas in text format (.txt). The pattern of text file is given in Example1.txt.
- 4) Choose your text file and click “fit”.
- 5) The result of regression analysis can be shown with the figure on the left window in 3-D diagram. The right figure shown 2-D graph of the survey data. In 3-D, you can change the direction by clicking left mouse. In 2-D, the yellow, green, and purple lines represent the subsidence profile, slope and curvature of the ground surface.
- 6) Box “Export” can be exported value of x, y, z and regression in text file.
- 7) Text box on the bottom of the window is the result of calculations. You have to use the value of S_{\max} and Slope max to calculate the solution cavern by “Predict Cavern.xls” program.

- 8) Open program “Predict Cavern.xls”.
- 9) Input the parameters S_{\max} , Slope max, Deformation modulus (E_m) and Friction angle (ϕ) (E_m and ϕ are obtained from laboratory or field testing).
- 10) The program gives the cavern depth (d), cavern diameter (w), roof deformation (R_s) and radius of influence ($B/2$) under sub-critical and critical conditions.

APPENDIX C

PUBLICATION

PUBLICATION

Aracheeploha, S., Horkaew, P. and Fuenkajorn, K. (2009). **Prediction of cavern configurations from subsidence data**, In *Proceedings of the Second Thailand Symposium on Rock Mechanics (ThaiRock 2009)*, Jomtien Palm Beach Hotel & Resort, Chonburi, 12-13 March 2009, pp. 161 – 176.

Prediction of cavern configurations from subsidence data

S. Archeeploha, P. Horkaew & K. Fuenkajorn

Geomechanics Research Unit, Suranaree University of Technology, Thailand

Keyword: Subsidence, brine, salt rock, cavern, sinkhole

ABSTRACT: An analytical method has been developed to predict the location, depth and size of caverns created at the interface between salt and overlying formations. A governing hyperbolic equation is used in a statistical analysis of the ground survey data to determine the cavern location, maximum subsidence, maximum surface slope and surface curvature under the sub-critical and critical conditions. The regression produces a set of subsidence components and a representative profile of the surface subsidence under sub-critical and critical conditions. Finite difference analyses using FLAC code correlate the subsidence components with the cavern size and depth under a variety of strengths and deformation moduli of the overburden. Set of empirical equations correlates these subsidence components with the cavern configurations and overburden properties. For the super-critical condition a discrete element method (using UDEC code) is used to demonstrate the uncertainties of the ground movement and sinkhole development resulting from the complexity of the post-failure deformation and joint movements in the overburden.

1 INTRODUCTION

Salt and associated minerals in the Khorat and Sakon Nakhon basins, northeast of Thailand have become important resources for mineral exploitation and for use as host rock for product storage. For over four decades, local people have extracted the salt by using an old fashioned technique, called here the 'brine-pumping' method. A shallow borehole is drilled into the rock unit directly above the salt. Brine (saline groundwater) is pumped through the borehole and left to evaporate on the ground surface. Relatively pure halite with slight amounts of associated soluble minerals is then obtained. This simple and low-cost method can however cause an environmental impact in the form of unpredictable ground subsidence, sinkholes and surface contamination (Fuenkajorn, 2002). Even though the brine pumping industry has been limited to strictly controlled areas, isolated from agricultural areas and farmlands, severe surface subsidence and sinkholes have commonly found outside the controlled areas, particularly on the upstream side of the groundwater flow (Figure 1).

The subsidence is caused by deformation or collapse of the cavern roof at the interface between the salt and overburden. Precise locations of the dissolved caverns are difficult to determine due to the complexity of groundwater circulation, infiltration of fresh surface water, brine pumping

Prediction of cavern configurations from subsidence data



Figure 1. Some sinkholes caused by brine pumping at Nonsabaeng village, Nongkwang, Banmuang district, Sakon Nakhon. (From Wannakao et al., 2004).

rates, and number and intensity of the pumping wells. As a result location and magnitude of the subsidence are very unpredictable. Exploratory drilling and geophysical methods (e.g., resistivity and seismic surveys) have normally been employed to determine the size, depth and location of the underground cavities in the problem areas in an attempt to backfill the underground voids, and hence minimizing the damage of the engineering structures and farmland on the surface (Jenkunawat, 2005, 2007; Wannakao, 2004, 2005). The geophysical and drilling investigations for such a widespread area are costly and time-consuming. This calls for a quick and low cost method to determine the size, depth and location of the solution caverns. The method should be used as an early warning tool so that mitigation can be implemented before the uncontrollable and severe subsiding of the ground surface occurs.

The objective of this research is to develop a method to predict the location, depth and size of solution caverns created at the interface between the salt and the overlying formation. The effort includes statistical analysis of the ground survey data in the subsiding areas, numerical simulations to correlate subsidence components with the overburden properties, cavern diameter and depth, and formulation of empirical relations between the cavern configurations and the subsidence components.

2 SITE CONDITIONS

Rock salt in the Maha Sarakham formation, northeast of Thailand is separated into 2 basins: the Sakon Nakhon basin and the Khorat basin. Both basins contain three distinct salt units: Upper, Middle and Lower members. Figure 2 shows a typical stratigraphic section of the Maha Sarakham formation. The Sakon Nakhon basin in the north covers an area of approximately 17,000 square kilometers. The Khorat basin in the south covers more than 30,000 square kilometers (Figure 3). Warren (1999) gives a detailed description of the salt and geology of the basins. From over 300 exploratory boreholes drilled primarily for mineral exploration, Suwanich (1978) estimates the geologic reserve of the three salt members from both basins as 18 MM tons. Vattanasak (2006) has re-compiled the borehole data and proposes a preliminary design for salt solution mining caverns based on a series of finite element analyses, and suggests that the inferred reserve for solution mining of the Lower Salt member of the Khorat basin is about 20 billion tons. This estimate excludes residential and national forest areas.

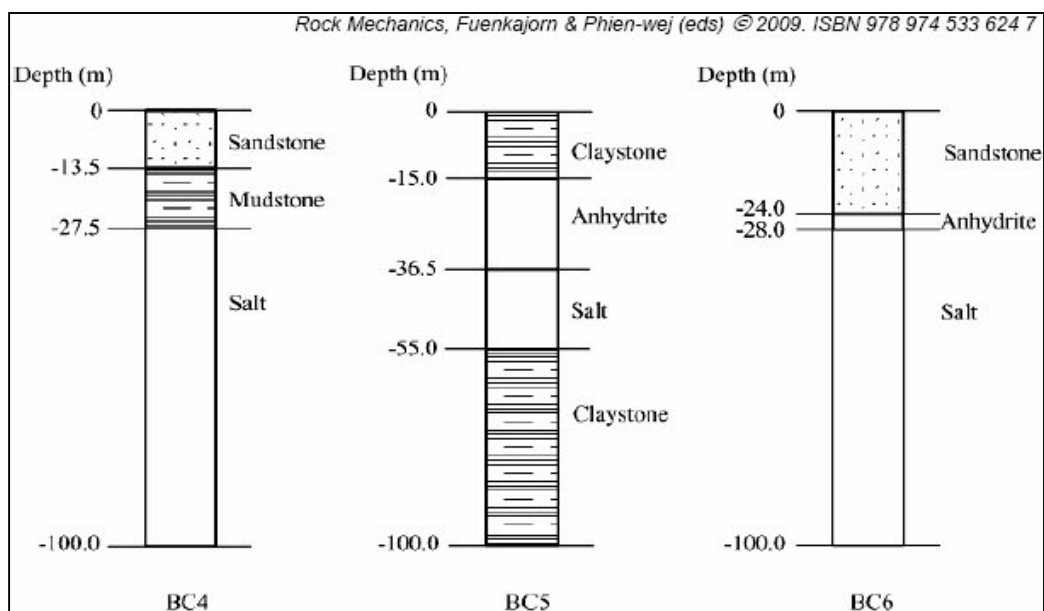


Figure 2. Stratigraphic units from some boreholes near brine pumping areas in the Sakon Nakhon basin (modified from Jenkunawat, 2005).

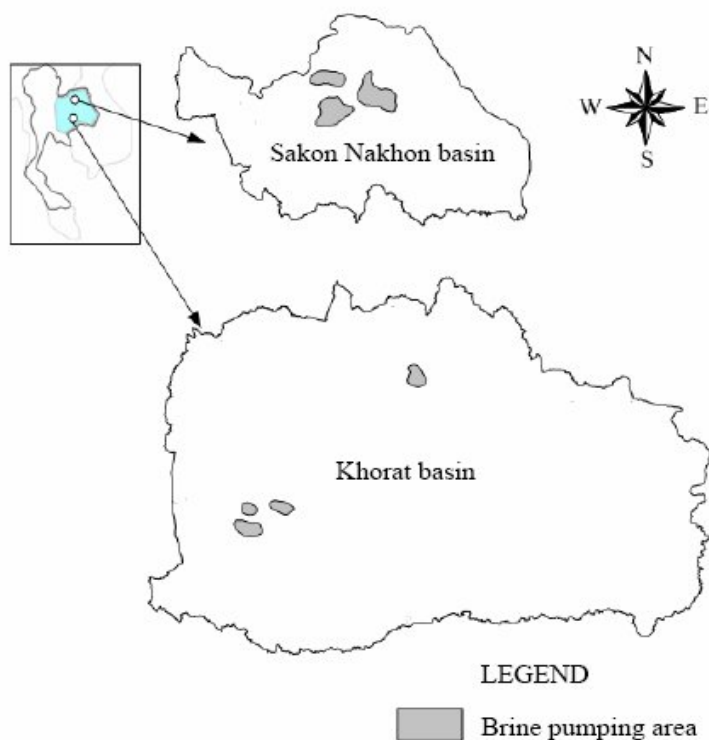


Figure 3. Brine pumping areas in Khorat and Sakon Nakhon salt basins.

Figure 3 also shows the areas where the brine pumping have been practices. Depths of the shallowest salt in those areas vary from 40 m to 200 m. It belongs to the Middle or Lower member, depending on locations. Most of the brine pumping practices are however in the areas where the topography is flat, groundwater table is near the surface, and the salt depth is less than 50 m in the Sakon Nakhon basin, and about 100 m in the Khorat basin (Jenkunawat, 2005; Wannakao, 2005). The overburden consists mainly of mudstone siltstone and sandstone of the Middle Clastic, and claystone and mudstone of the Lower Clastic, with fractures typically dipping less than 30 degrees, and rarely at 70 degrees (Crosby, 2007). The members are characterized by abundant halite and anhydrite-filled fractures and bands with typical thickness of 2 cm to 5 cm.

Direct shear tests performed in this research yield the cohesion and friction angle of 0.30 MPa and 27° for the smooth saw-cut surfaces prepared from the Middle Clastic siltstone. More mechanical properties for these clastic members are summarized by Wannakao et al. (2004) and Crosby (2007).

3 STATISTICAL ANALYSIS OF GROUND SURVEY DATA

A statistical method is developed to determine the maximum subsidence magnitude, maximum slope profile, curvature of the ground surface, and the cavern location. The regression is performed on the ground survey data obtained from subsiding areas. It is assumed here that the cavern model is a half-oval shaped with the maximum diameter, w , located at the contact between the salt and the overburden. The ground surface, overburden and salt are horizontal. Figure 4 identifies the variables used in this study. The radius of influence ($B/2$) represents the radius of the subsiding area where the vertical downward movement of the ground equals 1 cm or greater.

The survey data referred to here are the vertical displacements of the ground surface (z) measured at various points respected to a global x-y coordinate (Figure 5). A hyperbolic function modified from Singh (1992) is proposed to govern the characteristics of surface subsidence profile. It expresses the subsidence function, $S(r_i)$ (subsidence magnitude at point 'i', where i varied from 1 to the total number of measurements, n) as:

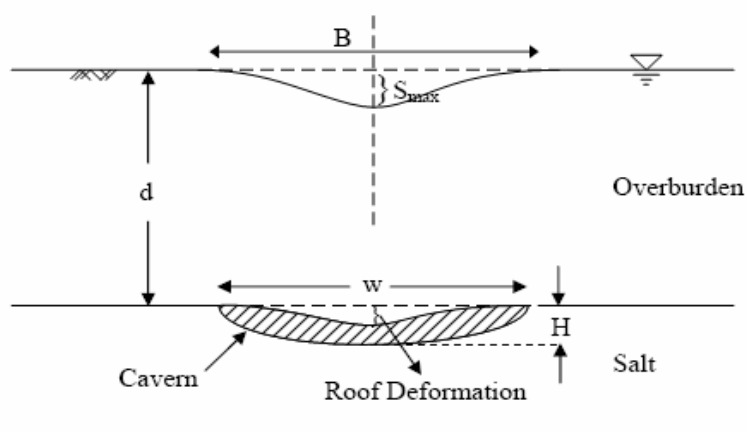


Figure 4. Variables used in this study.

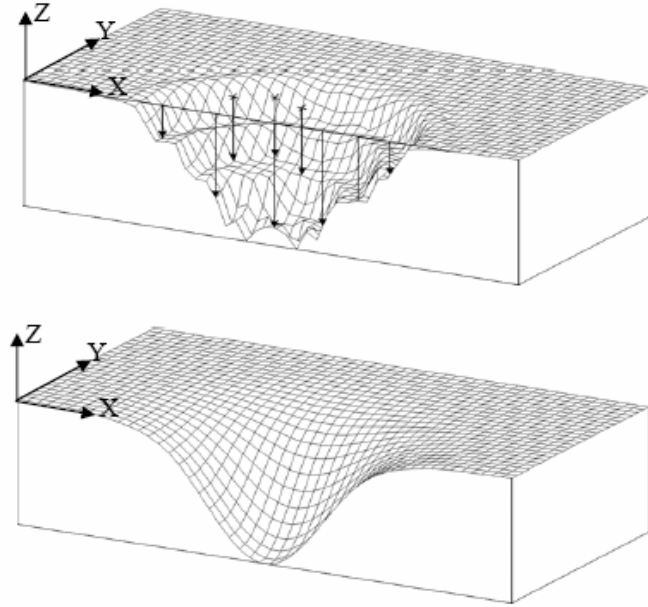


Figure 5. Regression of ground survey data (top) to obtain a representative hyperbolic profile of ground surface (bottom). Vertical scale is greatly exaggerated.

$$S(r_i) = a_0 \tanh(10a_1r_i - a_2) + a_3 \quad (i = 1, 2, 3, \dots, n) \quad (1)$$

$$\text{where } r_i = \sqrt{(x_i - a_4)^2 + (y_i - a_5)^2} \quad (2)$$

r_i = distance from data point 'i' to the center of the group of data,
 x_i, y_i = coordinates of subsidence measured at point 'i'
 a_0, a_1, a_2, a_3, a_4 and a_5 are constants related to the subsidence components and coordinates of the maximum subsidence location, which can be defined as:
 a_0 = half of the maximum subsidence (S_{\max}),
 a_1 = scaling factor,
 a_2 = planar offset,
 a_3 = vertical offset,
 $a_4 = \sum x_i / n$, and
 $a_5 = \sum y_i / n$.

Similarly the maximum slope (G) of the surface subsidence induced at the inflection point can be determined as:

$$G = S'(r_i) = 10a_0 \times a_1 \operatorname{sech}^2(10a_1r_i - a_2) \quad (3)$$

The maximum curvature (ρ) of the ground surface is calculated as:

$$\rho = S''(r_i) = -200a_0a_1^2 \operatorname{sech}^2(10a_1r_i - a_2) \times \tanh(10a_1r_i - a_2) \quad (4)$$

Prediction of cavern configurations from subsidence data

Regression analysis of the survey data using equation (1) will provide the three subsidence components and cavern location. These components will be correlated with the cavern depth and diameter in the following section. The regression also provides a smooth profile of the subsidence in three-dimension, as shown in Figure 5. Accuracy of the results depends on the number of the field measurements.

It is recognized that several theoretical models and governing equations have been developed to predict the subsiding characteristics of the ground surface induced by underground openings (e.g., Nieland, 1991; Shu and Bhattacharyya, 1993; Cui et al., 2000; Asadi et al., 2005). Singh (1992) also proposes several profile functions to represent the subsidence characteristics above mine openings. Singh's hyperbolic function is used here because it is simple and can provide results close to those obtained from numerical simulations (discussed in the next section).

4 FINITE DIFFERENCE SIMULATIONS

Finite difference analyses are performed to correlate the surface components with the cavern depth and diameter. The FLAC code (Itasca, 1992) is used here to simulate the subsidence magnitude, surface slope, cavern roof deformation and radius of influence on the surface. The variables include cavern diameter, cavern depth, and overburden mechanical properties. To cover the entire range of the cavern ground conditions, over 400 finite difference meshes have been constructed to represent cavern diameters (w) varying from 20 m to 100 m with an interval of 10 m, and the cavern depths (d) from 40, 60 to 80 m. Figure 6 gives an example of the computer model. The analysis is made in axial symmetry and under a hydrostatic stress field. The cavern is assumed to be half-oval shaped, and is under hydrostatic pressure of saturated brine. The groundwater table is assumed to be at the ground surface. The overburden is represented by a single unit of clastic rock with deformation moduli varying from 20, 40, 60 to 80 MPa, and internal friction angles from 20, 40 to 60 degrees. The cohesion equals zero in all cases. The mechanical properties of the clastic rock used here are within the range of those compiled by Thiel and Zabuski (1993).

After several trials the critical cavern diameters (the maximum diameter before failure occurs) can be determined along with their corresponding cavern depths, roof deformations, and mechanical properties of the overburden. This therefore represents the critical condition as defined by Singh (1992).

Figure 7 plots the maximum surface slope (G) normalized by the critical diameter (w_{crit}) as a function of the overburden friction angles (ϕ) for various deformation moduli (E_m). For each deformation modulus the normalized maximum slope (G/w_{crit}) increases with the friction angle, which can be represented by an exponential equation. Their empirical constants A_0 and B_0 depend on the deformation modulus. A power equation can be used to correlate A_0 and B_0 with the deformation modulus E_m , as shown in Figure 7. The normalized maximum slope can be expressed as:

$$G / w_{crit} = 0.0012 E_m^{-0.849} \exp(0.0103 \phi E_m^{0.27}) \quad (5)$$

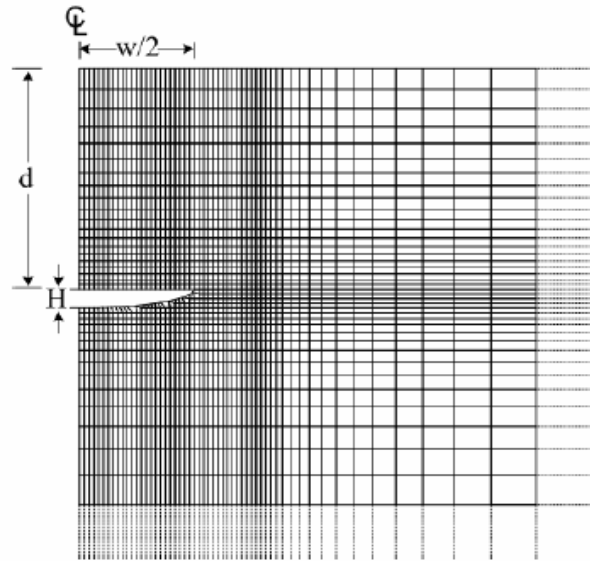
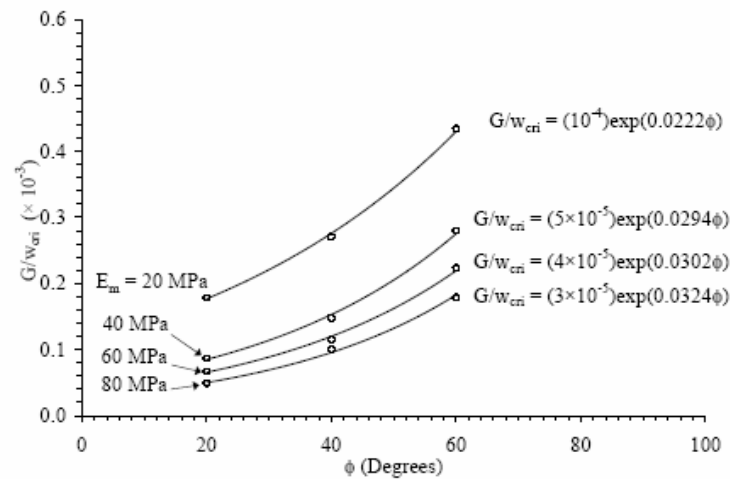


Figure 6. Example of finite difference mesh used in FLAC simulation. Analysis is made in axial symmetry. $H = 5$ m, $d = 60$ m, $w = 60$ m, $B = 172$ m, $E_m = 40$ MPa and $\phi = 20^\circ$.



$$G/w_{cri} = A_0 \cdot \exp(B_0 \phi), \text{ where; } A_0 = \alpha_{A0} \cdot E_m^{\beta_{A0}}, B_0 = \alpha_{B0} \cdot E_m^{\beta_{B0}}$$

| E_m (MPa) | A_0 | α_{A0} | β_{A0} | B_0 | α_{B0} | β_{B0} |
|-------------|--------------------|---------------|--------------|--------|---------------|--------------|
| 20 | 10^{-4} | 0.0012 | -0.849 | 0.0222 | 0.0103 | 0.27 |
| 40 | 5×10^{-5} | | | 0.0294 | | |
| 60 | 4×10^{-5} | | | 0.0302 | | |
| 80 | 3×10^{-5} | | | 0.0324 | | |

Figure 7. Maximum slope to critical cavern width ratio (G/w_{cri}) as a function of friction angle (ϕ) for various deformation moduli (E_m). A_0 , B_0 , α_{A0} , β_{A0} , α_{B0} and β_{B0} are empirical constants.

Prediction of cavern configurations from subsidence data

The cavern depth at the critical condition decreases with increasing deformation modulus (Figure 8). The depth normalized by the critical diameter (d/w_{cri}), can be expressed as a function of E_m as:

$$d/w_{\text{cri}} = (-0.0213\phi^{-0.636})E_m + 1.55\exp(-0.0163\phi) \quad (6)$$

Similar to the derivation above, the relationships for the vertical deformation of the cavern roof (R_s) and the radius of influence on the surface ($B/2$) can also be developed (Figures 9 and 10).

$$R_s/S_{\text{max,cri}} = (10^{-5}\phi - 0.0058)E_m - 0.0519\phi + 4.393 \quad (7)$$

$$B/w_{\text{cri}} = 0.11\exp(-0.058\phi)E_m + 2.844\exp(-0.0094\phi) \quad (8)$$

The same procedure is used for the sub-critical condition. The correlation results are shown in Figures 11 through 13, and can be expressed by the following equations:

$$G/w = 0.0012E_m^{-0.412} \cdot (S_{\text{max}}^{0.36E_m^{0.12}}) \quad (9)$$

$$d/w = (-0.0002E_m + 0.132)G^{(-0.7E_m^{-0.1743})} \quad (10)$$

$$R_s/w = (0.205E_m^{-0.701}) \cdot S_{\text{max}}^{(0.0432E_m^{0.386})} \quad (11)$$

The computer simulations are compared with those calculated by Singh's hyperbolic function for some cases in Figure 14. FLAC simulation gives the subsidence magnitudes about 10% greater than those from the hyperbolic function. The maximum surface slopes calculated from both methods are similar.

5 EXAMPLE OF CALCULATION

This section shows how to determine the cavern depth and diameter from an example set of survey data, as given in Table 1. Regression of these data using equation (1) results in a maximum subsidence at the center of the cavern equal to 0.46 m. Equation (3) determines the maximum slope at the inflection point as 0.013. This example assumes that the deformation modulus of the overburden is known and equal to 20 MPa, with a friction angle equal to 40°. This example assumes that the groundwater table is at the ground surface.

Under critical condition the cavern diameter and depth can be estimated from equations (5) through (7), as 54.6 m and 41.9 m. The roof deformation and radius of influence are 1.02 m and 59.2 m. If the ground is under sub-critical condition, the cavern diameter and depth are predicted as 55.6 m and 43.2 m, with the roof deformation and radius of influence equal to 1.25 m and 60.3 m. It can be seen that the solutions are not unique depending on whether the cavern is under sub-critical or critical condition. The cavern diameter, roof deformation and radius of influence can however be calculated if the cavern depth can be pre-defined. Within the brine pumping areas the depth of the cavern roof or of the overburden-salt interface can often be determined from interpolating or extrapolating from the existing drill holes or brine pumping wells.

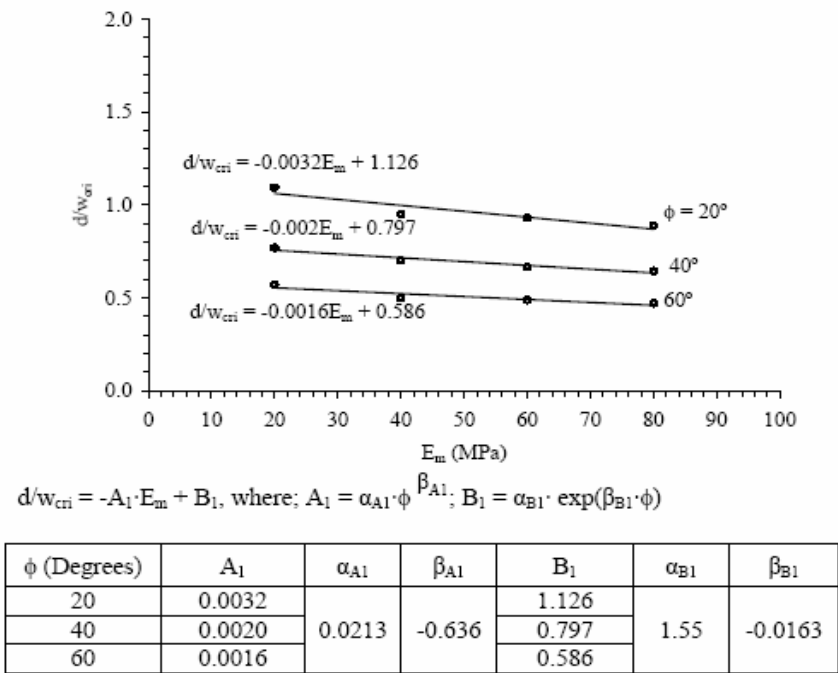


Figure 8. Cavern depth to critical cavern width ratio (d/w_{cri}) as a function of deformation modulus (E_m) for various friction angles (ϕ). A_1 , B_1 , α_{A1} , β_{A1} , α_{B1} and β_{B1} are empirical constants.

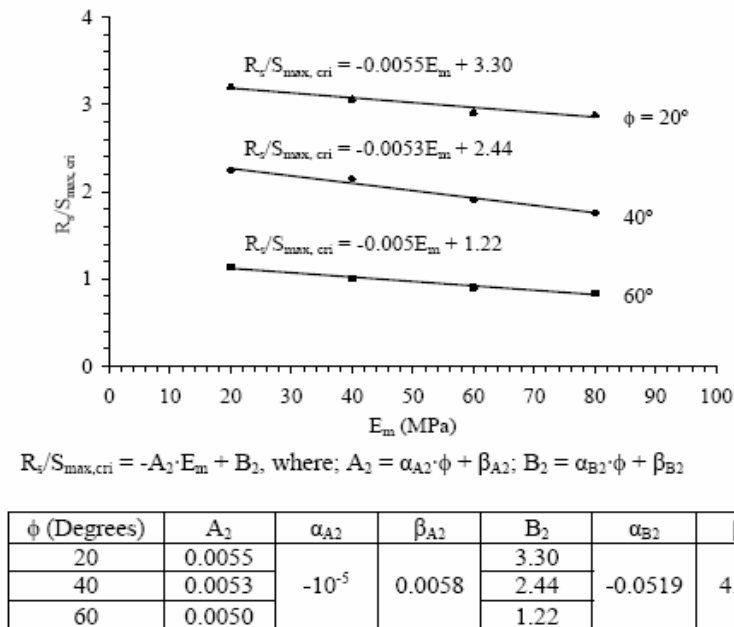
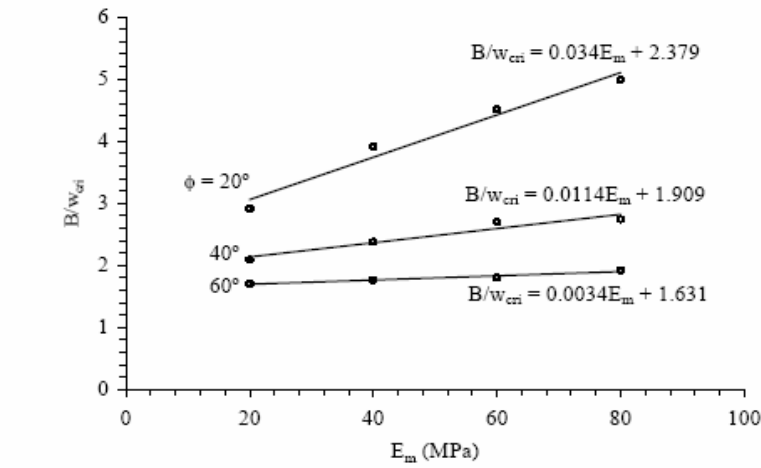


Figure 9. Roof deformation to maximum subsidence ratio at critical condition ($R_s/S_{max, cri}$) as a function of deformation modulus (E_m) for various friction angles. A_2 , B_2 , α_{A2} , β_{A2} , α_{B2} and β_{B2} are empirical constants.

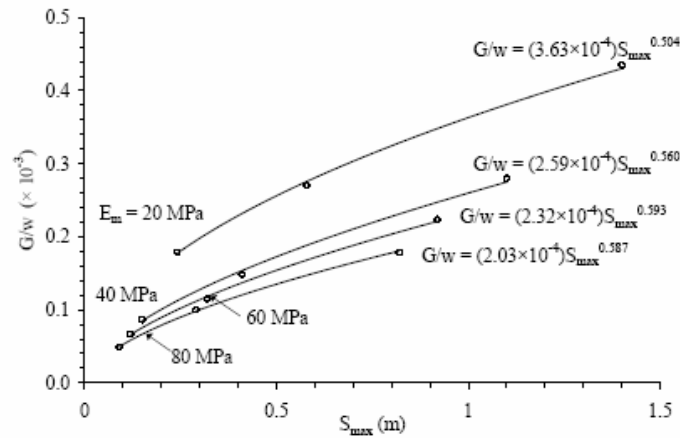
Prediction of cavern configurations from subsidence data



$$B/w_{cri} = A_3 \cdot E_m + B_3, \text{ where; } A_3 = \alpha_{A3} \cdot \exp(\beta_{A3} \cdot \phi); B_3 = \alpha_{B3} \cdot \exp(\beta_{B3} \cdot \phi)$$

| ϕ (Degrees) | A_3 | α_{A3} | β_{A3} | B_3 | α_{B3} | β_{B3} |
|------------------|--------|---------------|--------------|-------|---------------|--------------|
| 20 | 0.0340 | 0.11 | -0.058 | 2.379 | 2.844 | -0.0094 |
| 40 | 0.0114 | | | 1.909 | | |
| 60 | 0.0034 | | | 1.631 | | |

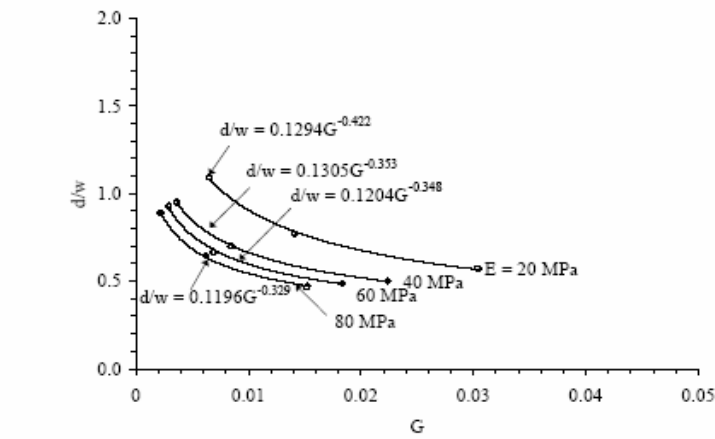
Figure 10. Diameter of influence to critical cavern width ratio (B/w_{cri}) as a function of deformation modulus (E_m) for various friction angles. A_3 , B_3 , α_{A3} , β_{A3} , α_{B3} and β_{B3} are empirical constants.



$$G/w = A_4 \cdot S_{max}^{B_4}, \text{ where; } A_4 = \alpha_{A4} \cdot E_m^{\beta_{A4}}, B_4 = \alpha_{B4} \cdot E_m^{\beta_{B4}}$$

| E_m (MPa) | A_4 | α_{A4} | β_{A4} | B_4 | α_{B4} | β_{B4} |
|-------------|-----------------------|---------------|--------------|-------|---------------|--------------|
| 20 | 3.63×10^{-4} | 0.0012 | -0.412 | 0.504 | 0.36 | 0.12 |
| 40 | 2.59×10^{-4} | | | 0.560 | | |
| 60 | 2.32×10^{-4} | | | 0.593 | | |
| 80 | 2.03×10^{-4} | | | 0.587 | | |

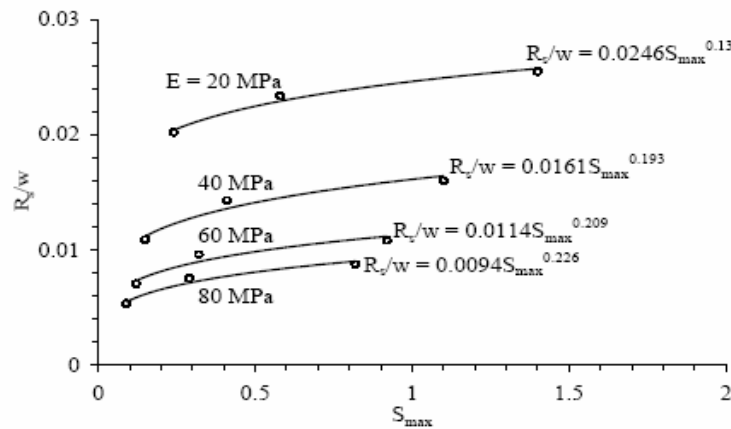
Figure 11. Maximum slope to cavern width ratio (G/w) as a function of maximum subsidence (S_{max}) for various deformation moduli (E_m). A_4 , B_4 , α_{A4} , β_{A4} , α_{B4} and β_{B4} are empirical constants.



$$d/w = A_5 \cdot G^{-B_5}, \text{ where: } A_5 = \alpha_{A5} \cdot E_m + \beta_{A5}; B_5 = \alpha_{B5} \cdot E_m + \beta_{B5}$$

| E_m (MPa) | A_5 | α_{A5} | β_{A5} | B_5 | α_{B5} | β_{B5} |
|-------------|--------|---------------|--------------|-------|---------------|--------------|
| 20 | 0.1294 | -0.0002 | 0.132 | 0.422 | 0.7 | -1.743 |
| 40 | 0.1305 | | | 0.353 | | |
| 60 | 0.1204 | | | 0.348 | | |
| 80 | 0.1196 | | | 0.329 | | |

Figure 12. Cavern depth to cavern width ratio (d/w) as a function of maximum slope (G) for various deformation moduli (E_m). A_5 , B_5 , α_{A5} , β_{A5} , α_{B5} and β_{B5} are empirical constants.



$$R_s/w = A_6 \cdot S_{\max}^{B_6}, \text{ where: } A_6 = \alpha_{A6} \cdot E_m + \beta_{A6}; B_6 = \alpha_{B6} \cdot E_m + \beta_{B6}$$

| E_m (MPa) | A_6 | α_{A6} | β_{A6} | B_6 | α_{B6} | β_{B6} |
|-------------|--------|---------------|--------------|-------|---------------|--------------|
| 20 | 0.0246 | 0.205 | -0.701 | 0.132 | 0.0432 | 0.386 |
| 40 | 0.0161 | | | 0.193 | | |
| 60 | 0.0114 | | | 0.209 | | |
| 80 | 0.0094 | | | 0.226 | | |

Figure 13. Ratio of roof deformation to cavern width ratio (R_s/w) as a function of maximum subsidence (S_{\max}) for various deformation moduli (E_m). A_6 , B_6 , α_{A6} , β_{A6} , α_{B6} and β_{B6} are empirical constants.

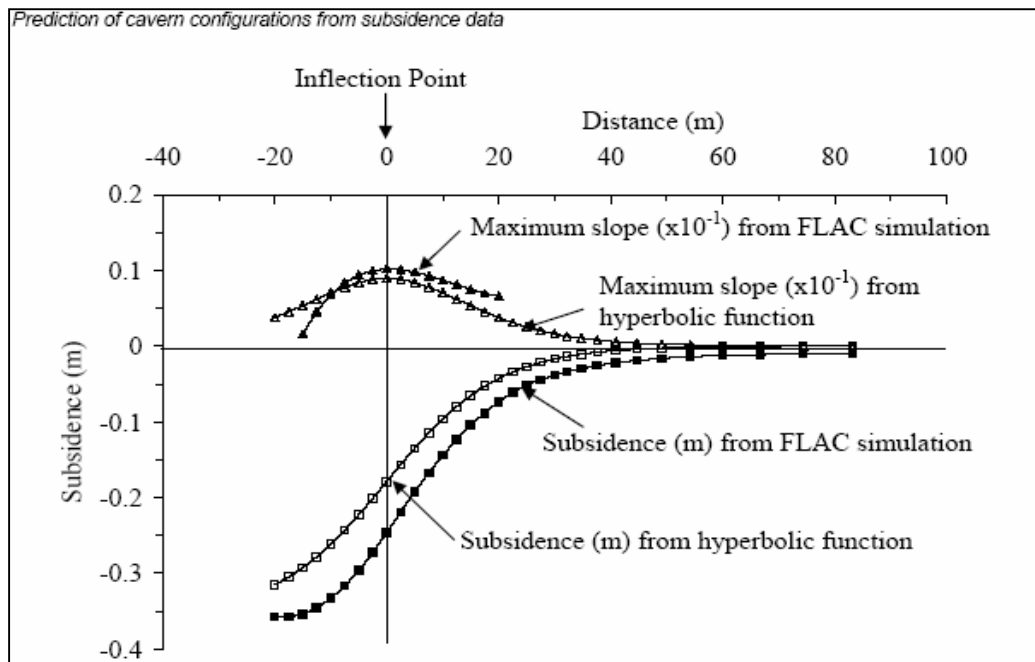


Figure 14. FLAC simulations compared with hyperbolic function calculations for $\phi = 20^\circ$, $E_m = 20$ MPa, $d = 40$ m and $w = 40$ m.

6 SUPER-CRITICAL CONDITION

Two scenarios can occur when the subsidence reaches its super-critical condition, which is dictated by the cavern height. If the cavern height is equal to or less than the roof deformation, the immediate roof rock will touch the cavern floor. Vertical movement of the ground may or may not continue depending on whether the salt floor dissolution is continued. In this case the subsidence is likely to be small, the subsiding area is relatively flat, and development of a sinkhole is unlikely.

If the cavern height is however significantly greater than the critical roof deformation, failure of the cavern roof can occur under the super-critical condition. The failure can progress upward and may lead to a sinkhole development. In this case the cavern location can be evidently defined, but accurate prediction of the cavern diameter and depth is virtually impossible. Subsurface investigations by Jenkunawat (2005) and Wannakao & Walsri (2007) reveals that collapsing of the roof rock above some caverns in a brine pumping area has also resulted in a large void remaining in the overburden.

7 DISCRETE ELEMENT ANALYSES

The difficulty in predicting the cavern configurations under super-critical condition is due to the complexity of the post failure behavior of the rock mass and movement of the joint system. To demonstrate these issues discrete element analyses are performed using UDEC code (Itasca, 2004) to simulate the movement of the jointed rock mass above an isolated salt cavern. The discrete element models are constructed to represent a cavern dissolved at the overburden-salt

Table 1. Example of ground survey data measured in subsiding area.

| i | x_i (m) | y_i (m) | z_i (m) | i | x_i (m) | y_i (m) | z_i (m) |
|----|-----------|-----------|-----------|----|-----------|-----------|-----------|
| 1 | 2.5 | 0.0 | -0.400 | 17 | 0.0 | 20.0 | -0.270 |
| 2 | -2.5 | 2.5 | -0.400 | 18 | 25.0 | 0.0 | -0.270 |
| 3 | 5.0 | 0.0 | -0.400 | 19 | 15.0 | 20.0 | -0.270 |
| 4 | 3.0 | 4.0 | -0.450 | 20 | -25.0 | 0.0 | -0.270 |
| 5 | -5.0 | 5.0 | -0.450 | 21 | 0.0 | 30.0 | -0.270 |
| 6 | 10.0 | 0.0 | -0.450 | 22 | 35.0 | 0.0 | -0.250 |
| 7 | 6.0 | 8.0 | -0.470 | 23 | 0.0 | 35.0 | -0.250 |
| 8 | -10.0 | 0.0 | -0.470 | 24 | 40.0 | 0.0 | -0.250 |
| 9 | -6.0 | 8.0 | -0.390 | 25 | 45.0 | 0.0 | -0.150 |
| 10 | 0.0 | 10.0 | -0.390 | 26 | 0.0 | 45.0 | -0.150 |
| 11 | 9.0 | 12.0 | -0.390 | 27 | -30.0 | 40.0 | -0.150 |
| 12 | 0.0 | 15.0 | -0.390 | 28 | -54.7 | 0.0 | -0.050 |
| 13 | -12.0 | 9.0 | -0.390 | 29 | 0.0 | 54.7 | -0.050 |
| 14 | 20.0 | 0.0 | -0.420 | 30 | 48.0 | 64.0 | -0.015 |
| 15 | 12.0 | 16.0 | -0.420 | 31 | 0.0 | 80.0 | -0.015 |
| 16 | -12.0 | 16.0 | -0.270 | 32 | -48.0 | 64.0 | -0.015 |

interface. The cavern depth, diameter and height are maintained constant at 40 m, 100 m and 30 m, representing a super-critical condition. A hydrostatic stress is applied on both sides of the model. For the first series of simulations there are two mutually perpendicular joint sets inclined at 45° , with friction angles varying from 20° , 30° and 40° . The second series assesses the effect of joint orientation by using a constant joint friction angle of 30° , and varying the joint orientations from 15° , 30° to 45° . The joint spacing for both cases is 8 m.

Simulation results from the first series (shown in Figure 15), suggest that even under the same cavern geometry and joint orientation, different joint friction angles can cause significantly different post-failure conditions. For the overburden with low-friction joints, the cavern can be completely filled with the collapsing rock blocks. This results in a deep sinkhole or a large depression area, or both. Gaps or voids can be formed if the overburden has joints with a higher friction angle, resulting in a shallower sinkhole and smaller subsiding area.

For the second series, Figure 16 compares the simulated results under the same joint friction ($\phi = 30^\circ$) but different joint angles. Different patterns of block collapsing can be obtained for the joints with 30° and 45° inclinations. It is interesting to observe that with the joint angle of 15° the roof failure does not progress upward, and has virtually no impact on the ground surface.

The numerical simulations under the assumed joint conditions above clearly demonstrate the complexity and uncertainty of the subsidence under super-critical condition which can not be easily determined by the analytical method proposed here. Detailed subsurface investigation is required to understand the failure and movement of the overburden under the super-critical condition.

Prediction of cavern configurations from subsidence data

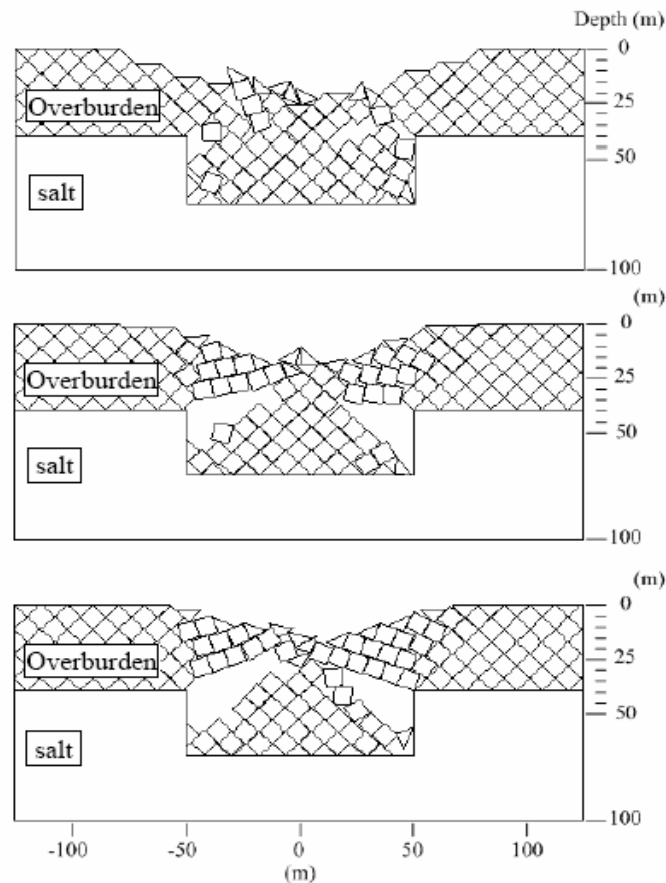


Figure 15. UDEC simulations for cavern roof failure for joints with friction angles of 20° (top), 30° (middle) and 40° (bottom). $H = 30$ m, $d = 40$ m, $w = 100$ m.

8 CONCLUSIONS

Regression analysis of the ground survey data can provide a smooth and representative profile of the surface subsidence which agrees reasonably well with the hyperbolic function proposed by Singh (1992). An analytical method developed from the results of finite difference analyses can be used to determine the cavern depth and diameter under sub-critical and critical conditions. Under which condition does the cavern belong to can be defined if the cavern depth is known, in most cases probably by interpolating between nearby boreholes or wells exploratory. The correlations of the subsidence components with the overburden mechanical properties and cavern geometry are applicable to the range of site conditions specifically imposed here (e.g., half oval-shaped cavern created at the overburden-salt interface, horizontal rock units, flat ground surface, and saturated condition). These relations may not be applicable to other subsidence induced under different rock characteristics or different configurations of the caverns. The proposed method is not applicable under super-critical conditions where post-failure behavior of the overburden rock mass is not only unpredictable but also complicated by the system of joints, as demonstrated by the results of the discrete element analyses. The proposed method is useful as a predictive tool to identify

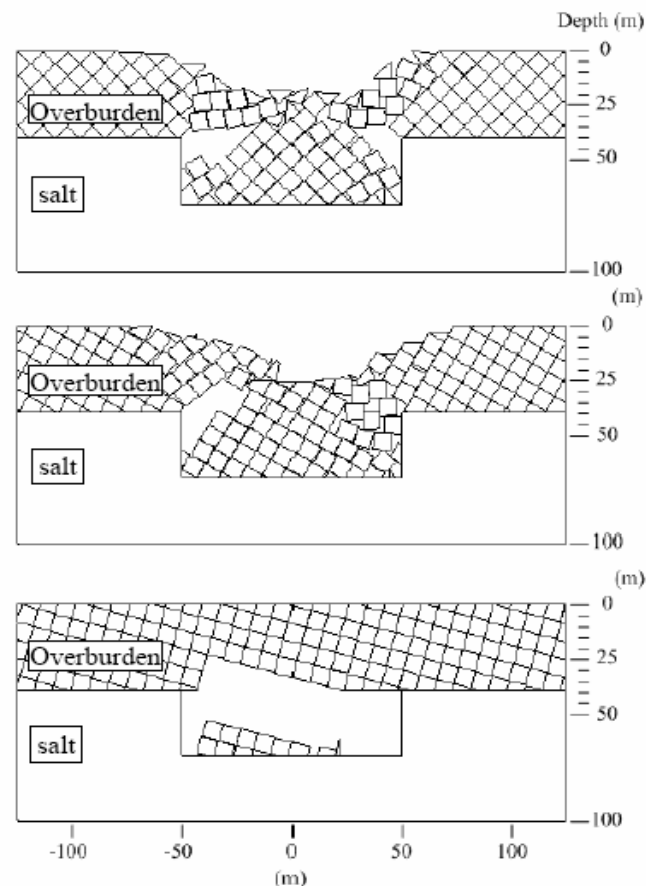


Figure 16. UDEC simulations for cavern roof failure with joint dip angles of 45° (top), 30° (middle) and 15° (bottom). $H = 30$ m, $d = 40$ m, $w = 100$ m.

the configurations of a solution cavern and the corresponding subsidence components induced by the brine pumping practices. Subsequently, remedial measure can be implemented to minimize the impact from the cavern development before severe subsidence or sinkhole occurs.

ACKNOWLEDGEMENT

The research is funded by Suranaree University of Technology. Permission to publish this paper is gratefully acknowledged.

REFERENCES

- Asadi, A., Shahriar, K., Goshtasbi, K., & Najm, K., 2005. Development of new mathematical model for prediction of surface subsidence due to inclined coal-seam mining. *Journal of the South African Institute of Mining and Metallurgy*. 105: 15-20.

- Crosby, K., 2007. Integration of rock mechanics and geology when designing the Udon South sylvinitic mine. In *Proceedings of the First Thailand Symposium on Rock Mechanics*, Nakhon Ratchasima: Suranaree University of Technology. pp. 3-22.
- Cui, X., Miao, X., Wang, J., Yang, S., Liu, H., Song, Y., Liu, H., & Hu, X., 2000. Improved prediction of differential subsidence caused by underground mining. *International Journal of Rock Mechanics and Mining Sciences*, Beijing: Pergamon Press, 37(4): 615-627.
- Fuenkajorn, K., 2002. Design guideline for salt solution mining in Thailand, *Research and Development journal of the Engineering Institute of Thailand*, pp. 1-8.
- Itasca, 1992. *User Manual for FLAC—Fast Lagrangian Analysis of Continua, Version 4.0*. Itasca Consulting Group Inc., Minneapolis, Minnesota.
- Itasca, 2004. *UDEC 4.0 GUI A Graphical User Interface for UDEC*. Itasca Consulting Group Inc., Minneapolis, Minnesota.
- Jenkunawat, P., 2005. Results of drilling to study occurrence of salt cavities and surface subsidence Ban Non Sabaeng and Ban Nong Kwang, Amphoe Ban Muang, Sakon Nakhon. *International Conference on Geology, Geotechnical and Mineral Resources of Indochina (GEOINDO 2005)*, Khon Kaen: Khon Kaen University. pp. 259-267.
- Jenkunawat, P., 2007. Results of drilling to study occurrence of salt cavities and surface subsidence Ban Non Sabaeng and Ban Nong Kwang, Sakon Nakhon. In *Proceedings of the First Thailand Symposium on Rock Mechanics*, Nakhon Ratchasima: Suranaree University of Technology. pp. 257-274.
- Nieland, J. D. (1991) *SALT SUBSID: A PC-Based Subsidence Model*, Research project report No.1991-2-SMRI, Solution Mining Research Institute.
- Shu, D.M., & Bhattacharyya, A.K., 1993. Prediction of sub-surface subsidence movements due to underground coal mining. *Geotechnical and Geological Engineering*. Springer Netherlands. 11(4): 221-234.
- Singh, M. M., 1992. Mine subsidence. *SME Mining Engineering Handbook*. Hartman, H.L. (ed). Society for mining metallurgy and exploration, Inc., Littleton: Colorado. pp. 938-971.
- Suwanich, P., 1978. Potash in northeastern of Thailand (in Thai). Economic Geology Document No. 22. Bangkok: Economic Geology, Division, Department of Mineral Resources.
- Thiel, K & Zabuski, L., 1993. Rock mass investigations in hydroengineering. *Comprehensive Rock Engineering*. Hudson, J.A. (ed). London: Pergamon Press, 3: 839-861.
- Vattanasak, H., 2006. *Salt reserve estimation for solution mining in the Khorat basin*, M.Eng. Thesis, Nakhon Ratchasima: Suranaree University of Technology.
- Wannakao, L. & Walsri, C., 2007. Subsidence models in salt production area. In *Proceedings of the First Thailand Symposium on Rock Mechanics*, Nakhon Ratchasima: Suranaree University of Technology. pp. 311-321.
- Wannakao, L., Janyakorn, S., Munjai, D., & Vorarat, A., 2004. *Geological and geotechnical properties analysis of overburden and salt formations in the northeast for surface subsidence model*, final research report, Department of Geotechnology, Khon Kaen University. (in Thai)
- Wannakao, L., Munjai, D., & Janyakorn, S., 2005. Geotechnical investigation of surface subsidence at Ban Non Sabaeng salt production area, Sakon Nakhon, Thailand. *International Conference on Geology, Geotechnical and Mineral Resources of Indochina (GEOINDO 2005)*. Khon Kaen: Khon Kaen University. pp. 282.
- Warren, J., 1999. *Evaporites: Their Evolution and Economics*, Oxford: Blackwell Science.

BIOGRAPHY

Mr. Sarayuth Aracheeploha was born on January 21, 1984 in Prachuapkhirkhan province, Thailand. He received his Bachelor's Degree in Engineering (Geotechnology) from Suranaree University of Technology in 2006. For his post-graduate, he continued to study with a Master's degree in the Geological Engineering Program, Institute of Engineering, Suranaree university of Technology. During graduation, 2006-2009, he was a part time worker in position of research assistant at the Geomechanics Research Unit, Institute of Engineering, Suranaree University of Technology. He has published two technical papers related to rock mechanics, titled "Prediction of cavern configurations from subsidence data" published in the Proceeding of the Second Thailand symposium on rock mechanics, Chonburi, Thailand; and Suranaree Journal of Science and Technology, Suranaree University of Technology, Nakhon Ratchasima, Thailand. For his work, he is a good knowledge in geomechanics theory and practice.